

ISTANBUL TECHNICAL UNIVERSITY ★ INSTITUTE OF SCIENCE AND TECHNOLOGY

**INVESTIGATION OF RESIDUAL STRAINS ON ARTERIAL WALL BY
OPTICAL METHODS**

**M.Sc. Thesis by
Gökhan BAYSAL**

Department : Mechanical Engineering

Programme : Solid Mechanics

JULY 2011

**INVESTIGATION OF RESIDUAL STRAINS ON ARTERIAL WALL BY
OPTICAL METHODS**

**M.Sc. Thesis by
Gökhan BAYSAL
(503091522)**

**Date of submission : 17 June 2011
Date of defence examination: 30 June 2011**

**Supervisor (Chairman) : Dr. Ergün BOZDAĞ (ITU)
Co- Supervisor : Dr. Emin SÜNBÜLOĞLU (ITU)
Members of the Examining Committee : Prof. Dr. Tuncer TOPRAK (ITU)
Prof. Dr. Civan IŞLAK (IU)
Prof. Dr. Naci KOÇER (IU)**

JULY 2011

İSTANBUL TEKNİK ÜNİVERSİTESİ ★ FEN BİLİMLERİ ENSTİTÜSÜ

**DAMAR DUVARINDAKİ ÖN BİRİM ŞEKİL DEĞİŞTİRMELERİN
OPTİK YÖNTEMLER KULLANILARAK İNCELENMESİ**

**YÜKSEK LİSANS TEZİ
Gökhan BAYSAL
(503091522)**

**Tezin Enstitüye Verildiği Tarih : 17 Haziran 2011
Tezin Savunulduğu Tarih : 30 Haziran 2011**

**Tez Danışmanı : Dr. Ergün BOZDAĞ (İTÜ)
Eş Danışman : Dr. Emin SÜNBÜLOĞLU (İTÜ)
Diğer Jüri Üyeleri : Prof. Dr. Tuncer TOPRAK (İTÜ)
Prof. Dr. Civan IŞLAK (İÜ)
Prof. Dr. Naci KOÇER (İÜ)**

TEMMUZ 2011

FOREWORD

First of all I would like to present my deep gratefulness to my “growing” family for their understanding and existance,

Mr. Emin SÜNBÜLOĞLU for his support, guidance and friendship during whole study and all studies on theoratical and experimental mechanics ,

Mr. Ergün BOZDAĞ for inviting me inside the doors of biomechanics, guiding me in various studies that we have conducted together and sharing ideas,

Mr. Tuncer TOPRAK for being there and giving all of us the power and the ambitiousness,

Mr. Civan IŞLAK for his valuable ideas about experimental setup and giving us the perspective on arterial biomechanics,

Mr. M. Aykut ANİK and Mr. Lazari KOZMANOĞLU for their help on providing specimens,

Mr. Orhan KAMBUROĞLU for his unbelievable talent and “precise” touch on all experimental setup of ours,

All colleagues for kindly supporting during rush times;

and

ITU Institute of Science and Technology for supporting this study.

July 2011

Gökhan BAYSAL

Mechanical Engineer

TABLE OF CONTENTS

	<u>Page</u>
TABLE OF CONTENTS	vii
ABBREVIATIONS	ix
LIST OF TABLES	xi
LIST OF FIGURES	xiii
SUMMARY	xv
ÖZET	xvii
1 INTRODUCTION	19
2 BASIC ARTERIAL ANATOMY and HISTOLOGY	21
2.1 Overview of the Arterial System.....	21
2.2 Arterial Histology	22
2.2.1 Components of arterial layers	23
2.2.1.1 Smooth muscles	23
2.2.1.2 Collagen fibers	24
2.2.1.3 Elastin.....	24
2.2.1.4 Ground substance.....	24
2.2.2 Layers.....	24
2.2.2.1 Tunica intima	25
2.2.2.2 Tunica media.....	25
2.2.2.3 Tunica adventitia.....	27
3 ARTERIAL WALL MECHANICS	29
3.1 Basic Algebra of Vectors and Tensors.....	29
3.1.1 Direct notation.....	29
3.1.2 Index notation.....	34
3.1.3 Coordinate transformations.....	40
3.1.4 Vectorial transformation law.....	41
3.1.5 Tensorial transformation law	42
3.1.6 Principal values	43
3.1.7 Principal scalar invariants	43
3.1.8 Further results in tensor calculus	44
3.2 Kinematics	45
3.3 Basic Mechanics of General Soft Tissues.....	51
3.3.1 Inhomogeneous structure	51
3.3.2 Nonlinear behavior.....	52
3.3.3 Viscoelasticity	53
3.3.4 Anisotropy.....	54
3.3.5 Strain rate insensitivity.....	55
3.3.6 Incompressibility.....	56
3.4 Mechanical Behaviour of Arterial Wall.....	56
3.4.1 Residual strains and stresses	57
3.4.1.1 Opening angle	58
3.4.1.2 Kinematics of the stress-relieving cut.....	59

3.4.1.3 Reverse Formulation	61
4 EXPERIMENTAL STUDIES	65
4.1 Digital Image Correlation.....	65
4.1.1 Background of DIC	65
4.1.1.1 Two dimensional (2D) DIC.....	66
4.1.1.2 Three dimensional (3D) DIC.....	67
4.1.2 Essential concepts	67
4.1.3 Intensity interpolation	68
4.1.4 Subset based image displacements and pattern development	69
4.1.5 3D Digital image correlation.....	69
4.2 3D DIC System Verification Tests.....	70
4.2.1 Verification test on mirrored-vision.....	70
4.2.2 Silicone bar and mechanical extensometer test.....	72
4.2.3 Underwater correlation accuracy tests	75
4.2.4 Opening Angle – Test on Engineering Silicone.....	77
4.2.5 Underwater arterial wall tests.....	80
5 CONCLUSION AND REMARKS.....	87
REFERENCES	89
CURRICULUM VITAE.....	93

ABBREVIATIONS

$\mathbf{u}, \mathbf{x}, \mathbf{X}, \mathbf{v}, \mathbf{w} \dots$: Vector
\mathbf{I}	: Identity tensor
\mathbf{O}	: Zero tensor
\mathbf{F}	: Deformation gradient tensor
\mathbf{U}	: Symmetric tensor, Right Cauchy stretch tensor
\mathbf{V}	: Left Cauchy stretch tensor
\mathbf{R}	: Orthogonal rotation tensor
\mathbf{W}	: Skew-symmetric tensor
\mathbf{C}	: Right Cauchy-Green deformation tensor
\mathbf{B}	: Left Cauchy-Green deformation tensor
\mathbf{E}	: Lagrangian strain tensor
\mathbf{e}	: Euler-almansi strain tensor
\mathbf{L}	: Velocity gradient tensor
\mathbf{D}	: Strain rate tensor
\mathbf{Q}	: Orthogonal tensor
$\hat{\mathbf{n}}_i$: Nonzero normalized eigenvector
\mathbf{e}_i	: Orthonormal basis vector
\mathbf{E}_A	: Orthonormal basis vector
\mathbf{T}	: Second order tensor
\mathbf{S}	: Second order tensor
i, j	: Index parameters
\times	: Cross product
\otimes	: Tensor product
\cdot	: Dot product
$T^{(n)}$: Traction vector
β_0	: Reference configuration
β_t	: Current configuration
J	: Volume ratio
Ω	: Current domain
Ω_o	: Reference domain
∇_o	: The referential del operator
\det	: Determinant operation
tr	: Trace
δ	: Kronecker delta
ε_{ijk}	: Permutation symbol
λ	: Stretch ratio, Eigenvalues
(r, θ, z)	: Cylindrical coordinates in reference configuration
(ρ, ν, ζ)	: Cylindrical coordinates in intermediate configuration

(R, Θ, Z) : Cylindrical coordinates in final configuration

LIST OF TABLES

	<u>Page</u>
Table 2.1: Percentage composition of the media and adventitia of several arteries at in vivo blood pressure. Adapted from [4].....	23
Table 2.2: Arterial system geometry [4]	28
Table 3.1: Mechanical properties [19], [5], [20] and associated biochemical data [21] of some representative organs mainly consisting of soft connective tissues	53
Table 4.1: Error values for silicone bar and mechanical extensometer test.....	74
Table 4.2: Stretch ratio results for silicon bar, depending on both theoretical results and camera data.....	80
Table 4.3: Initial diameter values and diameter and opening angle values at each ..	84
Table 4.4: Stretch ratio results for arterial wall, depending on both theoretical results and experimental results.....	85
Table 4.5: Strain results for arterial wall, depending on both theoretical results and experimental results.....	85

LIST OF FIGURES

	<u>Page</u>
Figure 2.1 : Graph showing the relationship between the characteristics of blood circulation and the structure of the blood vessels. Adopted from [2]... 21	21
Figure 2.2 : Vessels of the blood circulatory system. Adopted from [3]..... 22	22
Figure 2.3 : Diagrammatic model of the major components of a healthy elastic artery: intima, media and adventitia. Adopted from [8]. 26	26
Figure 3.1 : Vector u with its Cartesian components u_1, u_2, u_3 35	35
Figure 3.2 : Reference and deformed configurations of a body [16]..... 46	46
Figure 3.3 : Schematic representation of the polar decomposition of deformation gradient. Material element is first stretched by U and then rotated by R , or first rotated by R and then stretched by V [17]..... 48	48
Figure 3.4 : Tensile properties of elastine-rich canine nuchal ligament, collagen-rich sole tendon and intestinal smooth muscle [24]..... 52	52
Figure 3.5 : Load-extension curve of a tendon (a), Influence of the strain rate [45, 46]. 54	54
Figure 3.6 : Viscoelastic behavior: a) stress relaxation , b) creep, c) hysteresis [46, 47]. 54	54
Figure 3.7 : Tension-extension ratio relations of rabbit skin [49]. 55	55
Figure 3.8 : Tensile properties of articular cartilage. 55	55
Figure 3.9 : Tensile properties of lung parenchyma at different strain rates [48].... 56	56
Figure 3.10 : Schematic of the opening angle experiment which is used for assessing the residual strain in biological organs with approximately cylindrical geometry. [39]..... 58	58
Figure 3.11 : Kinematics of the arterial wall relative various configurations..... 59	59
Figure 3.12 : Schema of the different configurations 62	62
Figure 4.1 : Random pattern in an image [42]. 66	66
Figure 4.2 : Image in memory and image on screen respectively at initial time. 68	68
Figure 4.3 : Image in memory and image on screen respectively after motion. 68	68
Figure 4.4 : Mapping of sensor positions P and Q in reference subset to p and q in deformed subset [44]. 69	69
Figure 4.5 : Single camera system (a) vs. two camera system (b) for recovering third dimension. 70	70
Figure 4.6 : Setup for verification test on mirrored-vision. 71	71
Figure 4.7 : Shots from Vic-3D workspace while mirror correlation test 71	71
Figure 4.8 : Strain results for verification test on mirrored-vision. 72	72
Figure 4.9 : Setup for silicone bar and extansometer test; (a) General view for experimental setup. (b) Close view on specimen, mirror and mechanical extansometer. 73	73
Figure 4.10 : Test results for the silicone bar and mechanical extansometer test.... 74	74
Figure 4.11 : Steel plates fixed to the jaws of the caliper and speckles in detail..... 75	75
Figure 4.12 : Underwater image correlation test setup. 75	75

Figure 4.13 : Setup for underwater optical correlation test. (a) Initial view of speckled steel plates, (b) Speckled plates after sliding motion.....	76
Figure 4.14 : Displacement results of underwater correlation accuracy tests.....	76
Figure 4.15 : Strain results of underwater correlation accuracy tests.	77
Figure 4.16 : Shots from silicon bar bending tests.....	78
Figure 4.17 : Bended silicon bar, (a) close configuration and (b) open configuration.	78
Figure 4.18 : Strain results for the inner and outer surfaces of silicone bar.	79
Figure 4.19 : Example shots from stress relieving radial cut tests.....	80
Figure 4.20 : Shots from Vic-3D workspace during arterial wall correlation test....	81
Figure 4.21 : Example photos from the top of an ovine arterial wall specimen at different times.	82
Figure 4.22 : Mean Error – Time graph for inside of arterial wall	86
Figure 4.23 : Mean Error – Time graph for outside of arterial wall	86

INVESTIGATION OF RESIDUAL STRAINS ON ARTERIAL WALL BY OPTICAL METHODS

SUMMARY

Cardiovascular diseases are one of the most important threat to human life in civilized world. Therefore nowadays researchers are mainly concentrated on investigating healthy and pathological cases of cardiovascular system. While a part of reasearch proceed on biological and medical studies, simultaneously another part proceeds on the ever-growing mathematics, mechanics and information technologies. Developing and investigating mechanical and mathematical formulations entreating vasculature, became easier with the help of progression on computational and experimental systems.

The aim of this study to focus on residual strains which is agreed to be one of the main indicator of growth in arterial wall, which is a biological tissue, and compare and evaluate experimental result obtained by advanced optical measurement systems to the result of theoretical assumptions

In the scope of this study initially the basic anatomical and histological information about arteries is given.

This section is followed by the section on the mechanics of arterial wall. Kinematics are introduced and mathematical formulations are given for forward deformation. In addition to that reverse deformation formulations are also derived.

In the next chapter named experimental studies, firstly studies conducted on investigation of accuracy of optical correlation systems. Error values of each verification test are evaluated. Then, radial cuts are introduced to arterial wall segments and strains are measured on exterior surfaces.

In the last section the implications of the study is evaluated. Ways of developing-contributing this study in future studies are indicated.

At the end of the study a significant difference between theoretical and experimental results revealed. This results and implications of the study will surely trigger and contribute future studies on the subject.

DAMAR DUVARINDAKİ ÖN BİRİM ŞEKİL DEĞİŞTİRMELERİN OPTİK YÖNTEMLER KULLANILARAK İNCELENMESİ

ÖZET

Özellikle gelişmiş toplumlarda kalp ve damar hastalıkları insan hayatını tehdit eden en önemli unsurlardan biridir. Bu sebeple günümüzde araştırmacılar dolaşım sisteminin sağlıklı ve patolojik vaka durumları üzerine araştırmalarını arttırarak sürdürmektedirler. Araştırmaların bir kısmı biyoloji ve tıp disiplinleri konularında ilerlerken aynı zamanda matematik, mekanik ve bilgi teknolojileri alanlarında da çalışmalar devamlı gelişme göstermektedir. Hesaplama ve ölçüm imkanlarının çok hızlı gelişmesiyle beraber dolaşım sistemini konu alan matematik ve mekanik denklemlerin oluşturulması ve incelenmesi kolaylaşmıştır.

Bu çalışmanın amacı, damarın kendini yeniden modellemesi ve gelişim sürecinin bir göstergesi olduğu belirtilen ön birim şekil değiştirmelerin üzerinde durularak literatürde bulunan teorik ön birim şekil değiştirme kabulünün doğrudan gelişmiş optik ölçümler ile ortaya çıkan sonuçlar karşılaştırılması ve sonuçların değerlendirilmesidir.

Çalışma kapsamında öncelikle damar duvarının anatomik yapısı hakkında temel bilgiler verilmiştir.

Bu bölümü damar duvar mekaniğinin incelenmesi bölümü takip etmiştir. Damar kinematiğine girilmiş ve ileri yöndeki şekil değiştirmeler için matematik ifadeler verilmiştir. Bu ifadelere ek olarak tersine denklemler de elde edilmiştir.

Bir sonraki bölüm olan deneysel çalışmalar bölümünde ise öncelikle optik şekil değişimi ölçüm sistemlerinin doğrulukları üzerine çalışmalar yapılmıştır. Her bir testin hata miktarları değerlendirilmiştir. Damar duvarının ön birim şekil değiştirmelerinin ölçülebilmesi için bir deney düzeneği oluşturulmuş ve deneyler gerçekleştirilmiştir.

Son bölümde çalışmanın değerlendirilerek sonuç çıkarımları yapılmış, ilerleyen dönemlerde çalışmanın nasıl geliştirilebileceğine dair yorumlara yer verilmiştir.

Deneyler sonucunda doğrudan ölçüm sonuçlarıyla teorik sonuçlar arasında belirgin bir fark ortaya çıkmıştır. Ortaya konular bu fark ve çalışmanın çıktıları gelecekteki çalışmaları tetikleyecek ve katkı sağlayacak unsurlar olarak önem taşıyacaktır.

1 INTRODUCTION

Cardiovascular diseases are one of the most important threat to human life in civilized world. Therefore nowadays researchers are mainly concentrated on investigating healthy and pathological cases of cardiovascular system. While a part of research proceed on biological and medical studies, simultaneously another part of research on this subject proceeds on the ever-growing mathematics, mechanics and information technologies. Developing and investigating mechanical and mathematical formulations became easier with the help of progression on computational and measurement systems.

Residual stresses are the internal stresses supported by a body in an unloaded equilibrium configuration. Because residual stresses can significantly affect the mechanical behaviour of a component, the measurement of these stresses and the prediction of their effect on mechanical behaviour are important objectives in many engineering problems.

The presence of a residual stress field can have a major impact on a body's effective mechanical properties. Residual stress in biological tissues develops through growth, and is important to the mechanical function of the tissues [35].

The aim of this study to focus on residual strains which is agreed to be one of the main indicator of growth in arterial wall and also compare and evaluate experimental results obtained by advanced optical measurement systems to the result of theoretical assumptions

It has been known for at least 50 years that when a ring segment is cut from an artery and a radial cut is made in the ring, it uncoils like a watch spring. In 1983 Vaishnav and Vossoughi and Chuong and Fung noted that this implied the existence of circumferential residual strains and therefore stresses, which remained in the vessel even when it was free of all external loads and were revealed only when it was cut radially [56,57,58].

By stepwise removal of the inner or outer layers of the porcine carotid artery by matching frozen specimens, Greenwald et al. showed that the true stress-free state can only be reached by partial destruction of the vessel wall and that different layers of the wall may each have different zero-stress states. It was also found that enzymatic digestion of elastin reduces residual strains; whereas removal of collagen or destruction of vascular smooth muscle cells had little effect, and it was speculated that the relationship between opening angle, position and elastin content might be associated with nonhomogeneity in the structure and/or composition of the vessel wall [59].

Recently, Stergiopoulos et al. have studied the elastic properties of porcine aortic media and found a significant difference in the opening angles between the inner and outer halves of the media, having separated them by lathing frozen specimens. The strains required to reassemble the layers, assuming that each is in a state of zero-stress, depend not only on the mismatch of the opening angles but also on the difference between the arc lengths that are in contact before the layers were separated [60].

In the scope of this study initially the basic anatomical and histological information about arteries is given.

This section is followed by the section on the mechanics of arterial wall. Kinematics are introduced and mathematical formulations are given for forward deformation. In addition to that reverse deformation formulations are also derived.

In the next chapter named experimental studies, firstly studies conducted on investigation of accuracy of optical correlation systems. Error values of each verification test are evaluated. Then, radial cuts are introduced to arterial wall segments and strains are measured on exterior surfaces.

In the last section the implications of the study is evaluated. Ways of developing-contributing this study in future studies are indicated.

2 BASIC ARTERIAL ANATOMY AND HISTOLOGY

2.1 Overview of the Arterial System

The vasculature consists of a complex system of blood vessels which carry blood to and from various organs of the body. This complex system, which comprises arteries, arterioles, capillaries, venules and veins, may be classified by their sizes, function and proximity to the heart. In addition to histological changes in the arterial walls, the arterial blood pressure and speed of flow decrease and become more steady as the distance from the heart increases. This decrease corresponds to the reduction in the number of elastic fibers and the increase in the number of smooth muscle cells in the arteries. The graph illustrates the gradual changes in the structure of vessels and their biophysical properties [1].

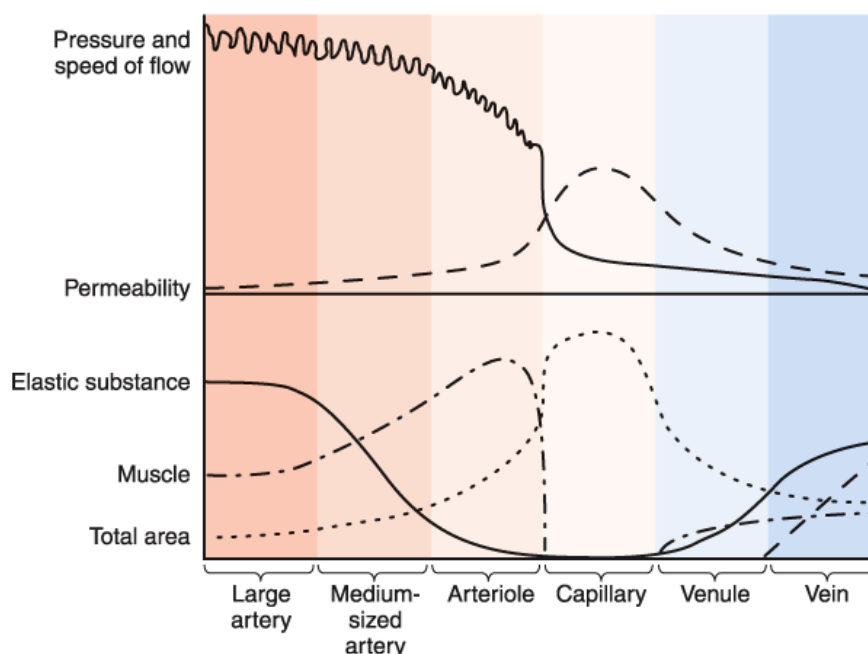


Figure 2.1 : Graph showing the relationship between the characteristics of blood circulation and the structure of the blood vessels. Adopted from [2].

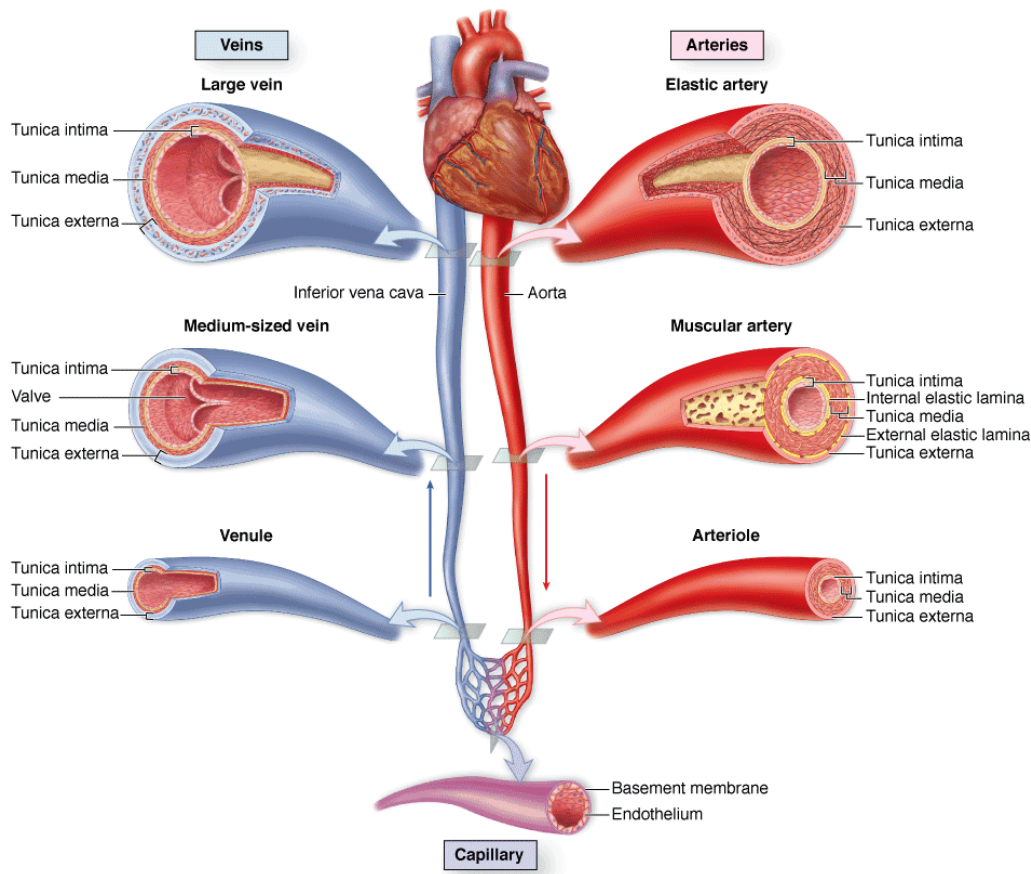


Figure 2.2 : Vessels of the blood circulatory system. Adopted from [3].

2.2 Arterial Histology

Commonly, arteries can be categorized according to two general types: elastic and muscular arteries. Elastic arteries tend to be larger- diameter vessels located close to the heart (for instance, the aorta, main pulmonary artery, common carotids and common iliacs), whereas muscular arteries smaller-diameter vessels located at the periphery (for instance, coronaries, cerebrals, femorals and renals). Nonetheless, transitional arteries exhibit morphological structures of both types. Approximate values for geometries of arteries can be found in Table 2.2 [4].

Table 2.1: Percentage composition of the media and adventitia of several arteries at in vivo blood pressure. Adapted from [5].

	Pulmonary artery	Thoracic aorta	Plantar artery
<i>Media</i>			
Smooth muscle	46.4 ± 7.7	33.5 ± 10.4	60.5 ± 6.5
Ground substance	17.2 ± 8.6	5.6 ± 6.7	26.4 ± 6.4
Elastin	9.0 ± 3.2	24.3 ± 7.7	1.3 ± 1.1
Collagen	27.4 ± 13.2	36.8 ± 10.2	11.9 ± 8.4
<i>Adventitia</i>			
Collagen	63.0 ± 8.0	77.7 ± 14.1	63.9 ± 9.7
Ground substance	25.1 ± 8.3	10.6 ± 10.4	24.7 ± 9.3
Fibroblasts	10.4 ± 6.1	9.4 ± 11.0	11.4 ± 2.6
Elastin	1.5 ± 1.5	2.4 ± 3.2	0

(Mean ± S.D.)

Regardless of type, all arterial walls are composed of three distinct layers, the intima (tunica intima), the media (tunica media) and the adventitia (tunica externa). The proportions of these three layers vary according to the size, location and function of the vessel. For example in large arteries number of lamellar layer increases with wall thickness and in smaller arteries the relative wall thickness is increased, elastin is less prominent in the media. In capillaries only the endothelium remains. Figure 2.2 shows vessels of the blood circulatory system which also includes a model of elastic artery.

Rest of the wall tissue, except layers listed above, consists of approximately 70% of water. There are four major components existing in layers: (also see Table 2.1)

2.2.1 Components of arterial layers

2.2.1.1 Smooth muscles

Smooth muscle cells, which are a living component of the walls of all vessels larger than capillaries, are arranged helically in layers. Each muscle cell is enclosed by an external lamina and by various amounts of other extracellular material, all of which these cells produce. under the neural control they actively contract and expand thus changing the geometry and elastic modulus of the tissue. Amount of muscles per unit volume in the wall increases as we move away from the heart and the small diameter arteries which are located close to the arterioles in which the muscles prevail are called muscular [3, 6].

2.2.1.2 Collagen fibers

Collagen are found throughout the wall: in the subendothelial layer, between muscle layers, and in the outer layers, is also a protein synthesized by smooth muscle cells and it has the appearance of nylon. Collagen fibers which are linked to each other give the tissue the required strength and integrity and prevent excess deformation. Collagen is inelastic, its modulus increases with increasing strain and is about 10 MPa to several hundred MPa [7]. Usually collagen is considered the factor which is responsible for the nonlinear elastic behavior of the tissue but the exact mechanisms of the Young modulus increase is not fully understood yet [6].

The ratio of elastin to collagen decreases as moved away of the heart, which is the reason why the arteries which are closer to the heart are called elastic ones in contrary to muscular arteries which are remote from the heart [3].

2.2.1.3 Elastin

Elastic material elastin, is a rubber-like protein, provides the flexibility for the vascular wall expanded under pressure. Elastin dominates in large arteries where it forms parallel lamellae regularly distributed between the muscle layers. Elastin is linear elastic with low elastic modulus (of order MPa, see [7]) and can sustain large stresses and strains (fibers may be stretched to 2.5 of their initial length) [3,6].

2.2.1.4 Ground substance

Scleroproteins and muscles are embedded in the Ground substance which forms a heterogeneous gel-like highly hydrated matrix in the extracellular spaces of the wall. It affects permeability and diffusion of substances through the wall. It consists of proteoglycans and is viscous, so it is usually considered not to contribute to elastic properties of the wall [3,6].

2.2.2 Layers

In the histological structure of the walls one can distinguish three layers called tunicae: Intima, media and adventitia.

2.2.2.1 Tunica intima

The intima is the innermost layer of the artery. It consists of thin monolayer of endothelial cells lining the arterial wall and underlying a thin basal lamina which is composed of a mesh like structure type IV collagen and the adhesion molecules fibronectin and laminin. There is also a subendothelial layer whose thickness varies with topography, age and disease. In healthy young muscular arteries, however, the subendothelial layer is almost nonexistent. In healthy young individuals the intima is very thin and makes an insignificant contribution to the solid mechanical properties of the arterial wall [4, 8,9].

In addition to being a nonthrombogenic layer between the blood and the contents of the vascular wall, the endothelium is very active biologically. It is known that pathological changes of the intimal components may be associated with atherosclerosis, the most common disease of arterial walls. It involves deposition of fatty substances, calcium, collagen fibers, cellular waste products and fibrin (a clotting material in the blood). The resulting build-up is called atherosclerotic plaque. It may be very complex in geometry and biochemical composition. In later stages the media is also affected. These pathological changes are associated with significant alterations in the mechanical properties of the arterial wall. Hence, the mechanical behavior of atherosclerotic arteries are significantly different from healthy arteries [6,8].

2.2.2.2 Tunica media

The media is the middle and the thickest layer of the artery and consists of a complex three-dimensional network of smooth muscle cells, and elastin and various types of collagen fibrils. In general, an artery contains proportionately more elastin the closer it is to the heart and more smooth muscle the farther away it is from the heart [9]. According to [10] the fenestrated elastic lamina separates the media into a varying number of well-defined concentrically fiber-reinforced medial layers. The number of elastic lamina decreases toward the periphery (as the size of the vessels decreases) so that elastic lamina is hardly present in muscular arteries.

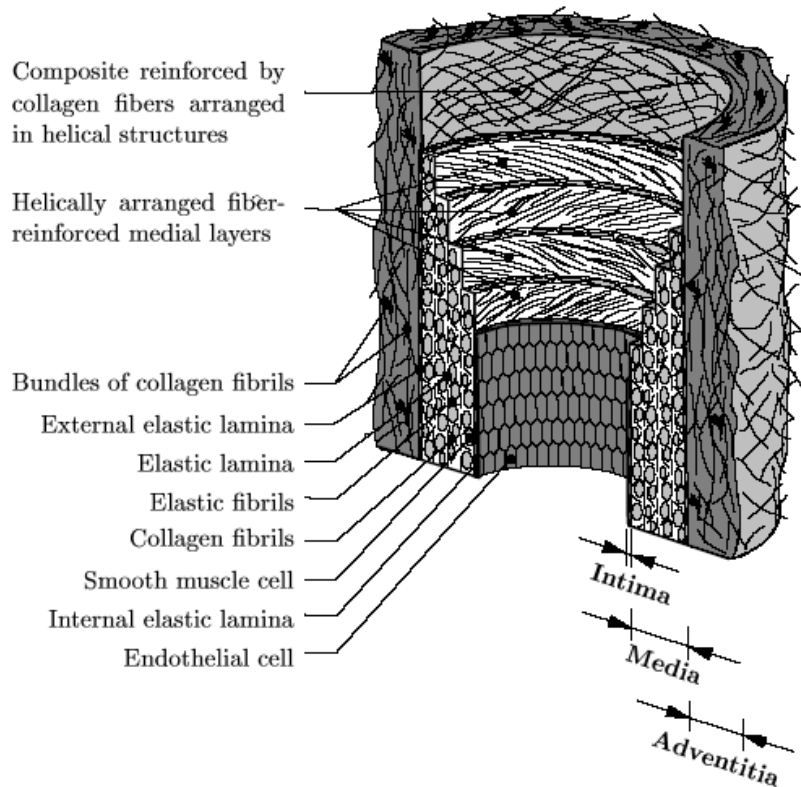


Figure 2.3 : Diagrammatic model of the major components of a healthy elastic artery: intima, media and adventitia. Adapted from [8].

The media is separated from the intima and adventitia by the so-called internal elastic lamina and external elastic lamina (absent in cerebral blood vessels), respectively. In muscular arteries these lamina appear as prominent structures, whereas in elastic arteries they are hardly distinguishable from the regular elastic lamina. The orientation of and close interconnection between the elastic and collagen fibrils, elastic lamina, and smooth muscle cells together constitute a continuous fibrous helix [11, 12].

The helix has a small pitch so that the fibrils in the media are almost circumferentially oriented. This structured arrangement gives the media high strength, flexibility and the ability to resist loads in both the longitudinal and circumferential directions. Smooth muscle hypertrophy, hyperplasia, apoptosis, and migration play essential roles in diseases such as atherosclerosis. Removal of matrix proteins, particularly of elastin, similarly plays a key role in aging and the progression of some diseases (e.g., abdominal aortic aneurysms) whereas an increased deposition of collagen plays a role

in diseases ranging from hypertension to atherosclerosis. From the mechanical perspective, the media is the most significant layer in a healthy artery [8,9].

2.2.2.3 Tunica adventitia

The adventitia is the outermost layer of the artery and consists mainly of fibroblasts and fibrocytes (cells that produce collagen and elastin), histological ground substance and thick bundles of collagen fibrils forming a fibrous tissue. The adventitia, which is thought to serve, in part, as a protective sheath that prevents acute overdistension of the media, is surrounded continuously by loose connective tissue. The thickness of the adventitia depends strongly on the type (elastic or muscular) and the physiological function of the blood vessel and its topographical site. For example, in cerebral blood vessels there is virtually no adventitia. The wavy collagen fibrils are arranged in helical structures and serve to reinforce the wall. Some investigators [13] consider its contribution to mechanical properties due to collagen fibres which stiffen and reinforce the wall as they straighten which prevents the whole artery from overextension and rupture. The elastic modulus of adventitia is commonly considered to be lower than that of media and consequently contribution of adventitia to the behavior of the wall is less than the middle layer [8,9].

Table 2.2: Arterial system geometry [4]

Blood vessel type	(Systemic) typical number	Internal diameter range	Length Range	Wall thickness
Aorta	1	1.0–3.0 cm	30–65 cm	2–3 mm
Pulmonary artery	-	2.5–3.1 cm	6–9 cm	2–3 mm
<i>Wall morphology (WM): Complete tunica adventitia, external elastic lamina, tunica media, internal elastic lamina, tunica intima, subendothelium, endothelium, and vasa vasorum vascular supply</i>				
Main branches	32	5 mm–2.25 cm	3.3–6 cm	≈ 2 mm
Large arteries	288	4.0–5.0 mm	1.4–2.8 cm	≈ 1 mm
<i>WM: A well-developed tunica adventitia and vasa vasorum, although wall layers are gradually thinning</i>				
Medium arteries	1152	2.5–4.0 mm	1.0–2.2 cm	≈ 0.75 mm
Small arteries	3456	1.0–2.5 mm	0.6–1.7 cm	≈ 0.50 mm
Tributaries	20736	0.5–1.0 mm	0.3–1.3 cm	≈ 0.25 mm
<i>WM: Well-developed tunica media and external elastic lamina, but tunica adventitia virtually nonexistent</i>				
Small rami	82944	250–500 μm	0.2–0.8 cm	≈ 125 μm
Terminal branches	497664	100–250 μm	1.0–6.0 mm	≈ 60 μm
<i>WM: A well-developed endothelium, subendothelium, and internal elastic lamina, plus about two to three 15-μm-thick concentric layers forming just a very thin tunica media; no external elastic lamina</i>				
Arterioles	18579456	25–100 μm	0.2–3.8 mm	≈ 20–30 μm
<i>WM: More than one smooth muscle layer (with nerve association in the outermost muscle layer), a well-developed internal elastic lamina; gradually thinning in 25- to 50-μm vessels to a single layer of smooth muscle tissue, connective tissue, and scant supporting tissue</i>				
Metarterioles	238878720	10–25 μm	0.1–1.8 mm	≈ 5–15 μm
<i>WM: Well-developed subendothelium; discontinuous contractile muscle elements; one layer of connective tissue</i>				
Capillaries	16124431360	3.5–10 μm	0.5–1.1 mm	≈ 0.5–1 μm
<i>WM: Simple endothelial tubes devoid of smooth muscle tissue; one-cell-layer-thick walls</i>				

3 ARTERIAL WALL MECHANICS

3.1 Basic Algebra of Vectors and Tensors

3.1.1 Direct notation

A vector is a mathematical quantity which possess characteristics of magnitude and direction. For this reason, vectors are often represented by arrows, the length of which denotes the magnitude [14]. In other words, a vector designated by \mathbf{u} , \mathbf{v} , \mathbf{w} is a directed line element in space. It is a model for physical quantities having both direction and length, for instance, force, velocity or acceleration. The two vectors that have the same direction and length are said to be equal [15].

The sum of vectors yields a new vector, based on the parallelogram law of addition. The following properties,

$$\mathbf{u} + \mathbf{v} = \mathbf{v} + \mathbf{u} , \quad (3.1)$$

$$(\mathbf{u} + \mathbf{v}) + \mathbf{w} = \mathbf{u} + (\mathbf{v} + \mathbf{w}) , \quad (3.2)$$

$$\mathbf{u} + \mathbf{0} = \mathbf{u} , \quad (3.3)$$

$$\mathbf{u} + (-\mathbf{u}) = \mathbf{0} , \quad (3.4)$$

Hold, where “ $\mathbf{0}$ ” denotes the unique zero vector with unspecified direction and zero length [15].

Besides addition and subtraction, which can be accomplished using the parallelogram law with the arrow representation, three “vector operations” of utmost importance are the scalar (or, dot) product,

$$\mathbf{u} \cdot \mathbf{v} = a \quad \text{where } a = |\mathbf{u}| \cdot |\mathbf{v}| \cdot \text{Cos}\theta . \quad (3.5)$$

The vector (or, cross) product,

$$\mathbf{u} \times \mathbf{v} = \mathbf{w} \text{ where } \mathbf{w} = |\mathbf{u}| \cdot |\mathbf{v}| \cdot \text{Sin}\theta \mathbf{e} \quad (3.6)$$

and the tensor (or, dyadic) product,

$$\mathbf{u} \otimes \mathbf{v} = \mathbf{T} \quad (3.7)$$

herein, θ is the angle between vectors \mathbf{u} and \mathbf{v} , $|\dots|$ denotes the magnitude of a vector, \mathbf{e} is a unit vector (i.e., $|\mathbf{e}|=1$) perpendicular to the plane containing \mathbf{u} and \mathbf{v} , \mathbf{T} is a second-order tensor. The magnitude of the vector \mathbf{w} is found by $|\mathbf{w}| = (\mathbf{w} \cdot \mathbf{w})^{\frac{1}{2}}$, and a unit vector \mathbf{e} in the direction of \mathbf{w} can be found via $\mathbf{e} = \frac{\mathbf{w}}{|\mathbf{w}|}$.

Two vectors, \mathbf{u} and \mathbf{v} are said to be orthogonal if $\mathbf{u} \cdot \mathbf{v} = \mathbf{0}$.

Collectively these equations above reveal that two vectors can “operate” on one another to yield a scalar, a new vector, or a second order tensor. Higher order tensors, as, for example, the third order tensor $\mathbf{u} \otimes \mathbf{v} \otimes \mathbf{w}$, can also be obtained [14].

Recall that the dot product commutes, that is

$$\mathbf{u} \cdot \mathbf{v} = \mathbf{v} \cdot \mathbf{u} \quad (3.8)$$

In contrast,

$$\mathbf{u} \times \mathbf{v} = -\mathbf{v} \times \mathbf{u} \quad (3.9)$$

and in general,

$$\mathbf{u} \otimes \mathbf{v} \neq \mathbf{v} \otimes \mathbf{u} \quad (3.10)$$

Also note that

$$(\mathbf{w} \otimes \mathbf{u}) \cdot \mathbf{v} = \mathbf{w}(\mathbf{u} \cdot \mathbf{v}) = a\mathbf{w} \quad (3.11)$$

$$\mathbf{w} \cdot (\mathbf{u} \otimes \mathbf{v}) = (\mathbf{w} \cdot \mathbf{u})\mathbf{v} = b\mathbf{v} \quad (3.12)$$

which shows, for example, that a “dot product” between a second-order tensor $\mathbf{w} \otimes \mathbf{u}$ and a vector \mathbf{v} , yields a vector in the direction of \mathbf{w} that has a different magnitude. Moreover, the “.” operation takes priority over the “ \otimes ”; thus the parenthesis can be

deleted. The last two equations reveal, therefore, that a second order tensor transforms a vector in to a new vector, that is why tensors are called linear transformations.

Many of the basic operations for second order tensors, say \mathbf{S} and \mathbf{T} , are similar to those for vectors. For instance, the basic associative and distributive laws for vectors are recalled,

$$(\mathbf{a}\mathbf{u}) \cdot \mathbf{v} = a(\mathbf{u} \cdot \mathbf{v}) = \mathbf{u} \cdot (\mathbf{a}\mathbf{v}) \quad (3.13)$$

$$(\mathbf{u} + \mathbf{v}) \cdot \mathbf{w} = \mathbf{u} \cdot \mathbf{w} + \mathbf{v} \cdot \mathbf{w} \quad (3.14)$$

These laws are similar for second order tensors, thus

$$(\mathbf{a}\mathbf{S}) \cdot \mathbf{v} = a(\mathbf{S} \cdot \mathbf{v}) = \mathbf{S} \cdot (\mathbf{a}\mathbf{v}) \quad (3.15)$$

and,

$$(\mathbf{S} + \mathbf{T}) \cdot \mathbf{v} = \mathbf{S} \cdot \mathbf{v} + \mathbf{T} \cdot \mathbf{v} \quad (3.16)$$

Satisfaction of these two equations ensures that the set of all second order tensors form a vector space. Which yields,

$$(\mathbf{a}\mathbf{u} + \mathbf{b}\mathbf{v}) \otimes \mathbf{w} = a(\mathbf{u} \otimes \mathbf{w}) + b(\mathbf{v} \otimes \mathbf{w}) \quad (3.17)$$

Additional operations important for second order tensors include the transpose $(\dots)^T$, trace $\text{tr}(\dots)$ and determinant $\det(\dots)$. In particular,

$$(\mathbf{u} \otimes \mathbf{v})^T = (\mathbf{v} \otimes \mathbf{u}) \quad (3.18)$$

which is to say that the transpose interchanges the order of the vectors that constitute the dyad, and

$$\text{tr}(\mathbf{u} \otimes \mathbf{v}) = \mathbf{u} \cdot \mathbf{v} \quad (3.19)$$

Which implies that the trace of a tensor yields the scalar product of the vectors constituting the dyad. Additionally;

$$\det \mathbf{T} = \det[\mathbf{T}] \quad (3.20)$$

where [...] denotes a matrix representation of \mathbf{T} . The determinant of a tensor thereby yields a scalar, one that equals the determinant of the matrix of components of the tensor. Another scalar measure of a second order tensor is its magnitude, given as

$$|\mathbf{T}| = \sqrt{\text{tr}(\mathbf{T}\mathbf{T}^T)} \quad (3.21)$$

A second order tensor, say $\mathbf{w} \otimes \mathbf{u}$, can also act on another second order tensor, say $\mathbf{v} \otimes \mathbf{x}$, to yield a second order tensor, viz.;

$$\mathbf{w} \otimes \mathbf{u} \cdot \mathbf{v} \otimes \mathbf{x} = (\mathbf{u} \cdot \mathbf{v}) \mathbf{w} \otimes \mathbf{x} = a (\mathbf{w} \otimes \mathbf{x}) \quad (3.22)$$

or either of two scalars,

$$\mathbf{w} \otimes \mathbf{u} : \mathbf{v} \otimes \mathbf{x} = (\mathbf{w} \cdot \mathbf{v})(\mathbf{u} \cdot \mathbf{x}) \quad (3.23)$$

or

$$\mathbf{w} \otimes \mathbf{u} \cdot \cdot \mathbf{v} \otimes \mathbf{x} = (\mathbf{w} \cdot \mathbf{x})(\mathbf{u} \cdot \mathbf{v}) \quad (3.24)$$

Note the order of these two operations, each of which is called a double-dot (or scalar) product. [14]

Other important relations involving the transpose are

$$(\mathbf{S} + \mathbf{T})^T = \mathbf{S}^T + \mathbf{T}^T \quad (3.25)$$

$$(\mathbf{S} \cdot \mathbf{T})^T = \mathbf{T}^T \cdot \mathbf{S}^T \quad (3.26)$$

$$(\mathbf{S}^T)^T = \mathbf{S}, \quad (3.27)$$

and likewise for the trace,

$$\text{tr}(a\mathbf{S} + b\mathbf{T}) = a\text{tr}(\mathbf{S}) + b\text{tr}(\mathbf{T}) \quad (3.28)$$

$$\text{tr}(\mathbf{S} \cdot \mathbf{T}) = \text{tr}(\mathbf{T} \cdot \mathbf{S}) \quad (3.29)$$

$$tr(\mathbf{S}^T) = tr(\mathbf{S}) \quad (3.30)$$

and for the determinant,

$$\det(a\mathbf{S}) = a^3 \det(\mathbf{S}) \quad (3.31)$$

$$\det(\mathbf{S}\cdot\mathbf{T}) = \det(\mathbf{S})\det(\mathbf{T}) \quad (3.32)$$

$$\det(\mathbf{S}^T) = \det(\mathbf{S}) \quad (3.33)$$

Here, it should be noted that a tensor is said to be symmetric or skew-symmetric if, respectively,

$$\mathbf{U} = \mathbf{U}^T, \quad \mathbf{W} = -\mathbf{W}^T. \quad (3.34)$$

Every skew-symmetric tensor \mathbf{W} has an associated axial vector \mathbf{w} such that $\mathbf{W}\cdot\mathbf{v} = \mathbf{w} \times \mathbf{v}$ for all vectors \mathbf{v} [14].

Moreover, every second order tensor \mathbf{T} can be written as the sum of a symmetric tensor \mathbf{U} and skew-symmetric tensor \mathbf{W} , that is,

$$\mathbf{T} = \mathbf{U} + \mathbf{W}, \quad \text{where } \mathbf{U} = \frac{1}{2}(\mathbf{T} + \mathbf{T}^T), \quad \mathbf{W} = \frac{1}{2}(\mathbf{T} - \mathbf{T}^T). \quad (3.35)$$

which yields;

$$tr(\mathbf{W}) = 0, \quad \det(\mathbf{W}) = 0. \quad (3.36)$$

The square, cube, etc. of a tensor are given by

$$\mathbf{S}^2 = \mathbf{S} \cdot \mathbf{S}, \quad \mathbf{S}^3 = \mathbf{S} \cdot \mathbf{S}^2 \quad (3.37)$$

There are two special second order tensors of importance, namely the zero tensor \mathbf{O} and the identity tensor \mathbf{I} , where

$$\mathbf{O} \cdot \mathbf{v} = \mathbf{o}, \quad \mathbf{I} \cdot \mathbf{v} = \mathbf{v}. \quad (3.38)$$

That is, the zero tensor transforms all vectors into the zero vectors and the identity tensor transforms all vectors into themselves. Likewise,

$$\mathbf{O} \cdot \mathbf{S} = \mathbf{O}, \quad \mathbf{I} \cdot \mathbf{S} = \mathbf{S}. \quad (3.39)$$

The trace and the determinant of the identity tensor arise often. They are given as

$$\text{tr}(\mathbf{I}) = 3, \quad \det(\mathbf{I}) = 1 \quad (3.40)$$

The inverse of a tensor $(\dots)^{-1}$ is defined by

$$\mathbf{S} \cdot \mathbf{S}^{-1} = \mathbf{I}, \quad \mathbf{S}^{-1} \cdot \mathbf{S} = \mathbf{I}. \quad (3.41)$$

Important relations for the inverse are

$$(a \cdot \mathbf{S})^{-1} = \frac{1}{a} \mathbf{S}^{-1} \quad (3.42)$$

$$(\mathbf{S} \cdot \mathbf{T})^{-1} = \mathbf{T}^{-1} \cdot \mathbf{S}^{-1} \quad (3.43)$$

Moreover, the transpose and determinant of the inverse of a tensor are given by

$$(\mathbf{S}^{-1})^T = (\mathbf{S}^T)^{-1}, \quad \det(\mathbf{S}^{-1}) = \frac{1}{\det \mathbf{S}}. \quad (3.44)$$

Note, too, that $(\mathbf{S}^{-1})^T$ is often denoted by \mathbf{S}^{-T} .

Finally, a second order tensor \mathbf{Q} is called orthogonal if

$$\mathbf{Q} \cdot \mathbf{Q}^T = \mathbf{Q}^T \cdot \mathbf{Q} = \mathbf{I} \quad (3.45)$$

That is, if its inverse equals its transpose. Also, the equations 3-32, 3-33 and 3-40 reveal that

$$\det(\mathbf{Q}) = \pm 1 \quad (3.46)$$

An orthogonal tensor is said to be proper if $\det(\mathbf{Q}) = 1$ [14].

3.1.2 Index notation

So far algebra has been presented in symbolic notation exclusively employing bold face letters. It represents a very convenient and concise tool to manipulate most of the relations used in continuum mechanics. However, particularly in computational

mechanics, it is essential to refer vector (and tensor) quantities to a basis. Additionally, to gain more insight in some quantities and to carry out mathematical operations among tensors more readily it is often helpful to refer to components [15].

In order to present coordinate expressions relative to a right-handed and orthonormal system, a fixed set of three basis vectors $\mathbf{e}_1, \mathbf{e}_2, \mathbf{e}_3$, (sometimes introduced as i, j, k) called a (Cartesian) basis, with properties is introduced.

$$\mathbf{e}_1 \cdot \mathbf{e}_2 = \mathbf{e}_1 \cdot \mathbf{e}_3 = \mathbf{e}_2 \cdot \mathbf{e}_3 = 0, \quad \mathbf{e}_1 \cdot \mathbf{e}_1 = \mathbf{e}_2 \cdot \mathbf{e}_2 = \mathbf{e}_3 \cdot \mathbf{e}_3 = 1 \quad (3.47)$$

These vectors of unit length which are mutually orthogonal form a so-called orthonormal system. Then any vector \mathbf{u} in the three-dimensional Euclidean space is represented uniquely by a linear combination of the basis vectors $\mathbf{e}_1, \mathbf{e}_2, \mathbf{e}_3$, i.e.

$$\mathbf{u} = u_1 \mathbf{e}_1 + u_2 \mathbf{e}_2 + u_3 \mathbf{e}_3 \quad (3.48)$$

where the three real numbers u_1, u_2, u_3 are the uniquely determined Cartesian components of vector \mathbf{u} along the given directions $\mathbf{e}_1, \mathbf{e}_2, \mathbf{e}_3$, respectively.

Using index notation the vector \mathbf{u} can be written as $\mathbf{u} = \sum_{i=1}^3 u_i \mathbf{e}_i$ or in an abbreviated form by leaving out the summation symbol, simply as

$$\mathbf{u} = u_i \mathbf{e}_i, \quad (\text{sum over } i=1,2,3). \quad (3.49)$$

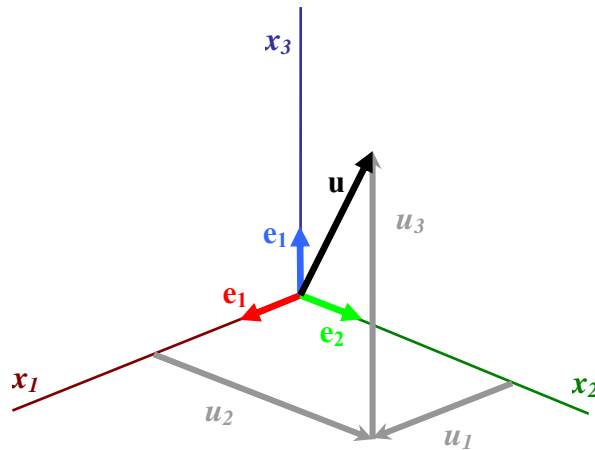


Figure 3.1 : Vector \mathbf{u} with its Cartesian components u_1, u_2, u_3 .

The summation convention says that whenever an index is repeated (only once) in the same term, then, a summation over the range of this index is implied unless otherwise indicated [15].

The index i that is summed over is said to be a dummy index, since a replacement by any other symbol does not affect the value of the sum. An index that is not summed over in a given term is called a free index. Note that in the same equation an index is either dummy or free. Thus, these relations can be written in a more convenient form as

$$\mathbf{e}_i \cdot \mathbf{e}_j = \delta_{ij} \equiv \begin{cases} 1, & \text{if } i = j \\ 0, & \text{if } i \neq j \end{cases} \quad (3.50)$$

which defines the Kronecker delta δ_{ij} . The useful properties are

$$\delta_{ii} = 3, \quad \delta_{ij} u_i = u_j, \quad \delta_{ij} \delta_{jk} = \delta_{ik}. \quad (3.51)$$

Taking the basis $\{\mathbf{e}_i\}$ and the equations above, the component expression for the dot product gives,

$$\mathbf{u} \cdot \mathbf{v} = u_i \mathbf{e}_i \cdot v_j \mathbf{e}_j = u_i v_j \mathbf{e}_i \cdot \mathbf{e}_j = u_i v_j \delta_{ij} = u_i v_i \quad (3.52)$$

$$\mathbf{u} \cdot \mathbf{v} = u_1 v_1 + u_2 v_2 + u_3 v_3 \quad (3.53)$$

In an analogous manner, the component expression for the square of the length of \mathbf{u} , is

$$|\mathbf{u}|^2 = u_1^2 + u_2^2 + u_3^2 \quad (3.54)$$

The cross product of \mathbf{u} and \mathbf{v} , denoted by $\mathbf{u} \times \mathbf{v}$ produces a new vector. In order to express the cross product in terms of components the permutation symbol is introduced as,

$$\varepsilon_{ijk} = \begin{cases} 1, & \text{for even permutations of } (i, j, k) \\ -1, & \text{for odd permutations of } (i, j, k) \\ 0, & \text{if there is a repeated index} \end{cases} \quad (3.55)$$

Consider the right-handed and orthonormal basis $\{ e_i \}$, then

$$\mathbf{e}_1 \times \mathbf{e}_2 = \mathbf{e}_3, \quad \mathbf{e}_2 \times \mathbf{e}_3 = \mathbf{e}_1, \quad \mathbf{e}_3 \times \mathbf{e}_1 = \mathbf{e}_2, \quad (3.56)$$

$$\mathbf{e}_2 \times \mathbf{e}_1 = -\mathbf{e}_3, \quad \mathbf{e}_3 \times \mathbf{e}_2 = -\mathbf{e}_1, \quad \mathbf{e}_1 \times \mathbf{e}_3 = -\mathbf{e}_2 \quad (3.57)$$

$$\mathbf{e}_1 \times \mathbf{e}_1 = \mathbf{e}_2 \times \mathbf{e}_2 = \mathbf{e}_3 \times \mathbf{e}_3 = \mathbf{0} \quad (3.58)$$

or in more convenient short-hand notation

$$\mathbf{e}_i \times \mathbf{e}_j = \varepsilon_{ijk} \mathbf{e}_k \quad (3.59)$$

Then the cross product of \mathbf{u} and \mathbf{v} yields,

$$\mathbf{w} = \mathbf{u} \times \mathbf{v} = u_i \mathbf{e}_i \times v_j \mathbf{e}_j = u_i v_j (\mathbf{e}_i \times \mathbf{e}_j) = \varepsilon_{ijk} u_i v_j \mathbf{e}_k = w_k \mathbf{e}_k \quad (3.60)$$

Recall the components of the resultant vector \mathbf{u} relative to the coordinate axes. That is,

$$\mathbf{u} = u_1 \mathbf{e}_1 + u_2 \mathbf{e}_2 + u_3 \mathbf{e}_3 = u_1 \mathbf{e}_1 + u_2 \mathbf{e}_2 + u_3 \mathbf{e}_3 \quad (3.61)$$

This equation also reveals that any vector can be represented in terms of linearly independent vectors. Likewise, any-second order tensor can be represented in terms of linearly independent dyads, as, for example, $\mathbf{e}_1 \otimes \mathbf{e}_1, \mathbf{e}_1 \otimes \mathbf{e}_2, \dots$ in Cartesian components. Hence, for the second-order tensor \mathbf{T} we can write

$$\begin{aligned} \mathbf{T} = & T_{11} \mathbf{e}_1 \otimes \mathbf{e}_1 + T_{12} \mathbf{e}_1 \otimes \mathbf{e}_2 + T_{13} \mathbf{e}_1 \otimes \mathbf{e}_3 \\ & + T_{21} \mathbf{e}_2 \otimes \mathbf{e}_1 + T_{22} \mathbf{e}_2 \otimes \mathbf{e}_2 + T_{23} \mathbf{e}_2 \otimes \mathbf{e}_3 \\ & + T_{31} \mathbf{e}_3 \otimes \mathbf{e}_1 + T_{32} \mathbf{e}_3 \otimes \mathbf{e}_2 + T_{33} \mathbf{e}_3 \otimes \mathbf{e}_3 \end{aligned} \quad (3.62)$$

where T_{11}, T_{12} , etc. are said to be components of \mathbf{T} relative to Cartesian axes. The equation 3.62 can be written in the more compact Einstein summation convention as

$$\mathbf{T} = T_{ij} \mathbf{e}_i \otimes \mathbf{e}_j \quad (3.63)$$

where the subscripts i and j are both repeated, that is "dummy." Note, too, the nine components of \mathbf{T} with respect to a Cartesian coordinate system, say T_{mn} , can easily be determined, viz.,

$$T_{mn} = \mathbf{e}_m \cdot (T_{ij} \mathbf{e}_i \otimes \mathbf{e}_j) \cdot \mathbf{e}_n \quad (3.64)$$

$$T_{mn} = T_{ij} (\mathbf{e}_m \cdot \mathbf{e}_i) (\mathbf{e}_j \cdot \mathbf{e}_n) \quad (3.65)$$

$$T_{mn} = T_{ij} \delta_{mi} \delta_{jn} \quad (3.66)$$

wherein the scalar components T_{ij} are considered before performing the dot products (on vectors); the replacement property of the Kronecker delta is thus revealed again. Because a second-order tensor has nine components, they can also be written in the form of a 3 x 3 matrix as

$$T_{ij} = [\mathbf{T}] = \begin{bmatrix} T_{11} & T_{12} & T_{13} \\ T_{21} & T_{22} & T_{23} \\ T_{31} & T_{32} & T_{33} \end{bmatrix} \quad (3.67)$$

A familiar example of matrix representation is the identity tensor \mathbf{I} , which has components

$$[\mathbf{I}] = \begin{bmatrix} 1 & 0 & 0 \\ 0 & 1 & 0 \\ 0 & 0 & 1 \end{bmatrix} \quad (3.68)$$

Relative to Cartesian coordinate axes. Thus, recalling the definition of Kronecker delta, we see the Kronecker delta simply represents the components of \mathbf{I} relative to Cartesian coordinate system. That is, we can write

$$\mathbf{I} = \delta_{ij} \mathbf{e}_i \otimes \mathbf{e}_j \quad (3.69)$$

Cartesian component representations for vectors and tensors reveal that the transformation of a vector into another vector via a second-order tensor simply involves a scalar product between appropriate bases:

$$(T_{ij}\mathbf{e}_i \otimes \mathbf{e}_j) \cdot (\mathbf{v}_k \mathbf{e}_k) = T_{ij} v_k \mathbf{e}_i (\mathbf{e}_j \cdot \mathbf{e}_k) \quad (3.70)$$

$$(T_{ij}\mathbf{e}_i \otimes \mathbf{e}_j) \cdot (\mathbf{v}_k \mathbf{e}_k) = T_{ij} v_k \mathbf{e}_i (\delta_{jk}) \quad (3.71)$$

$$(T_{ij}\mathbf{e}_i \otimes \mathbf{e}_j) \cdot (\mathbf{v}_k \mathbf{e}_k) = T_{ij} v_k \mathbf{e}_i \quad (3.72)$$

$$(T_{ij}\mathbf{e}_i \otimes \mathbf{e}_j) \cdot (\mathbf{v}_k \mathbf{e}_k) = u_i \mathbf{e}_i \quad (3.73)$$

Wherein we again used the replacement property of the Kronecker delta and let u_i represent the term(s) $T_{i1}v_1 + T_{i2}v_2 + T_{i3}v_3$.

A special vector called the del operator, which relative to Cartesian coordinates is defined by

$$\nabla = \mathbf{e}_i \frac{\partial}{\partial x_i} \quad (3.74)$$

and by using equation 3.74, , the gradient of a scalar a ,

$$\nabla a = \mathbf{e}_i \frac{\partial}{\partial x_i} (a) = \frac{\partial a}{\partial x_i} \mathbf{e}_i \quad (3.75)$$

The divergence and gradient of a vector \mathbf{u} , that is,

$$\nabla \cdot \mathbf{u} = \mathbf{e}_i \frac{\partial}{\partial x_i} \cdot (u_j \mathbf{e}_j) = \mathbf{e}_i \cdot \left(\frac{\partial u_j}{\partial x_i} \mathbf{e}_j + u_j \frac{\partial \mathbf{e}_j}{\partial x_i} \right) = \frac{\partial u_j}{\partial x_i} (\mathbf{e}_i \cdot \mathbf{e}_j) = \frac{\partial u_i}{\partial x_i}, \quad (3.76)$$

and

$$\nabla \mathbf{u} = \mathbf{e}_i \frac{\partial}{\partial x_i} \cdot (u_j \mathbf{e}_j) = \frac{\partial u_j}{\partial x_i} \mathbf{e}_i \otimes \mathbf{e}_j \quad (3.77)$$

or the divergence tensor \mathbf{T} ,

$$\nabla \cdot \mathbf{T} = \mathbf{e}_k \frac{\partial}{\partial x_k} \cdot (T_{ij} \mathbf{e}_i \otimes \mathbf{e}_j) \quad (3.78)$$

$$\nabla \cdot \mathbf{T} = \frac{\partial T_{ij}}{\partial x_k} (\mathbf{e}_k \cdot \mathbf{e}_i) \mathbf{e}_j = \frac{\partial T_{ij}}{\partial x_i} \mathbf{e}_j \quad (3.79)$$

Hence, $\nabla \cdot \mathbf{u}$ yields a scalar, ∇a and $\nabla \cdot \mathbf{T}$ yield vectors, and $\nabla \mathbf{u}$ yields a tensor [14].

Another convention arises naturally when one takes a derivative with respect to a vector.

$$\frac{\partial a}{\partial \mathbf{x}} \equiv \frac{\partial a}{\partial x_i} \mathbf{e}_i \quad (3.80)$$

and

$$\frac{\partial \mathbf{u}}{\partial \mathbf{x}} = \frac{\partial (u_i \mathbf{e}_i)}{\partial \mathbf{x}} = \frac{\partial (u_i \mathbf{e}_i)}{\partial x_j} \otimes \mathbf{e}_j = \frac{\partial u_i}{\partial x_j} \mathbf{e}_i \otimes \mathbf{e}_j \quad (3.81)$$

Derivatives with respect to a second-order tensor follow a similar convention:

$$\frac{\partial a}{\partial \mathbf{T}} = \frac{\partial a}{\partial T_{ij}} \mathbf{e}_i \otimes \mathbf{e}_j \quad (3.82)$$

The scalar products between two second-order tensors are

$$\mathbf{T} : \mathbf{S} = (T_{ij} \mathbf{e}_i \otimes \mathbf{e}_j) : (S_{mn} \mathbf{e}_m \otimes \mathbf{e}_n) \quad (3.83)$$

$$\mathbf{T} : \mathbf{S} = T_{ij} S_{mn} (\mathbf{e}_i \cdot \mathbf{e}_m) (\mathbf{e}_j \cdot \mathbf{e}_n) \quad (3.84)$$

$$\mathbf{T} : \mathbf{S} = T_{ij} S_{mn} \delta_{im} \delta_{jn} \quad (3.85)$$

$$\mathbf{T} : \mathbf{S} = T_{ij} S_{ij} \quad (3.86)$$

For which an alternative representation is

$$\mathbf{T} : \mathbf{S} = tr(\mathbf{T} \cdot \mathbf{S}^T) = tr(\mathbf{T}^T \cdot \mathbf{S}) \quad (3.87)$$

3.1.3 Coordinate transformations

It is worthwhile to mention that vectors and tensors themselves remain invariant upon a change of basis they are said to be independent of any coordinate system. However,

their respective components do depend upon the coordinate system introduced, which is arbitrary. The components change their magnitudes by a rotation of the basis vectors, but are independent of any translation [15].

If the transformation laws for various components of vectors and tensors under a change of basis is arranged;

$$\tilde{\mathbf{e}}_i = \mathbf{Q}\mathbf{e}_i \quad \text{and} \quad \mathbf{e}_i = \mathbf{Q}^T\tilde{\mathbf{e}}_i, \quad i = 1,2,3, \quad (3.88)$$

where \mathbf{Q} denotes the orthogonal tensor, with components Q_{ij} which are the same in either basis. The components describe the orientation of the two sets of basis vectors relative to each other. In particular, \mathbf{Q} rotates the basis vectors \mathbf{e}_i in to $\tilde{\mathbf{e}}_i$, while \mathbf{Q}^T rotates $\tilde{\mathbf{e}}_i$ back to \mathbf{e}_i . Using equations 3-63, 3-12 and 3-51 we find that

$$\mathbf{Q}\mathbf{e}_i = Q_{ji}\mathbf{e}_j \quad \text{and} \quad \mathbf{Q}^T\tilde{\mathbf{e}}_i = Q_{ij}\tilde{\mathbf{e}}_j \quad (3.89)$$

By comparing the equations above the orthogonality condition of the cosines may be extracted, characterized by $\mathbf{Q}^T\mathbf{Q} = \mathbf{Q}\mathbf{Q}^T = \mathbf{I}$. Equivalently, expressed in index or matrix notation

$$Q_{ij}Q_{ik} = Q_{ji}Q_{ki} = \delta_{jk}, \quad [\mathbf{Q}^T][\mathbf{Q}] = [\mathbf{Q}][\mathbf{Q}^T] = [\mathbf{I}] \quad (3.90)$$

Where $[\mathbf{Q}]$ contains the collection of the components Q_{ij} . It is an orthogonal matrix which is referred to as the transformation matrix. Note that $[\mathbf{Q}]^T = [\mathbf{Q}^T]$. In order to maintain the right-handedness of the basis vectors only rotations of the basis vectors has been admitted, consequently $\det[\mathbf{Q}] = \pm 1$.

3.1.4 Vectorial transformation law

When any vector \mathbf{u} resolved along the two sets $\{\tilde{\mathbf{e}}_i\}$ and $\{\mathbf{e}_i\}$ of basis vectors is considered, i.e.

$$\tilde{u}_i = \mathbf{u} \cdot \tilde{\mathbf{e}}_i \quad \text{in} \quad \{\tilde{\mathbf{e}}_i\} \quad (3.91)$$

$$u_i = \mathbf{u} \cdot \mathbf{e}_i \quad \text{in} \quad \{\mathbf{e}_i\} \quad (3.92)$$

Thus vectorial transformation law for the Cartesian components of the vector \mathbf{u} can be obtained, i.e.

$$\tilde{u}_i = \mathbf{u} \cdot \tilde{\mathbf{e}}_i = Q_{ji} (\mathbf{u} \cdot \mathbf{e}_j) = Q_{ji} u_j \quad \text{or} \quad (3.93)$$

$$[\tilde{\mathbf{u}}] = [\mathbf{Q}]^T [\mathbf{u}] \quad (3.94)$$

in analogous manner

$$u_i = Q_{ji} \cdot \tilde{u}_j \quad \text{or} \quad [\mathbf{u}] = [\mathbf{Q}][\tilde{\mathbf{u}}] \quad (3.95)$$

These equations determine the relationship between the components of a vector associated with the (old) basis $\{\mathbf{e}_i\}$ and the components of the same vector associated with another (new) basis $\{\tilde{\mathbf{e}}_i\}$ [15].

3.1.5 Tensorial transformation law

To determine the transformation laws for the Cartesian components of any second-order tensor \mathbf{A} , its components along the sets $\{\tilde{\mathbf{e}}_i\}$ and $\{\mathbf{e}_i\}$ of basis vectors are described, i.e.

$$\tilde{A}_{ij} = \tilde{\mathbf{e}}_i \cdot \mathbf{A} \tilde{\mathbf{e}}_j \quad \text{in} \quad \{\tilde{\mathbf{e}}_i\} \quad (3.96)$$

$$A_{ij} = \mathbf{e}_i \cdot \mathbf{A} \mathbf{e}_j \quad \text{in} \quad \{\mathbf{e}_i\} \quad (3.97)$$

Combining the equations above with 3-96 and 3-88, then the components A_{ij} , \tilde{A}_{ij} are related via the so-called tensorial transformation law [15].

$$\tilde{A}_{ij} = \tilde{\mathbf{e}}_i \cdot \mathbf{A} \tilde{\mathbf{e}}_j = (Q_{ki} \mathbf{e}_k) \cdot \mathbf{A} (Q_{mj} \mathbf{e}_m) \quad (3.98)$$

$$\tilde{A}_{ij} = Q_{ki} Q_{mj} (\mathbf{e}_k \cdot \mathbf{A} \mathbf{e}_m) \quad (3.99)$$

$$\tilde{A}_{ij} = Q_{ki} Q_{mj} A_{km} \quad \text{or} \quad [\tilde{\mathbf{A}}] = [\mathbf{Q}]^T [\mathbf{A}] [\mathbf{Q}] \quad (3.100)$$

Transformation $[\tilde{\mathbf{A}}] = [\mathbf{Q}]^T [\mathbf{A}] [\mathbf{Q}]$ relates different matrices $[\tilde{\mathbf{A}}]$ and $[\mathbf{A}]$, which have the components of the same tensor \mathbf{A} . Similarly, one can derive;

$$A_{ij} = Q_{ki}Q_{jm}\tilde{A}_{km} \quad \text{or} \quad [\mathbf{A}] = [\mathbf{Q}]^T[\tilde{\mathbf{A}}][\mathbf{Q}] \quad (3.101)$$

3.1.6 Principal values

The scalars λ_i characterize eigenvalues (principal values) of a tensor \mathbf{A} if there exist corresponding nonzero normalized eigenvectors $\hat{\mathbf{n}}_i$ of \mathbf{A} , so that

$$\mathbf{A}\hat{\mathbf{n}}_i = \lambda_i\hat{\mathbf{n}}_i, \quad (i = 1, 2, 3; \text{no summation}) \quad (3.102)$$

To identify the eigenvectors of a tensor, subsequently a hat on the vector quantity concerned, is used, for example $\hat{\mathbf{n}}$.

Thus, a set of homogeneous algebraic equations for the unknown eigenvalues λ_i , $i = 1, 2, 3$, and the unknown eigenvectors $\hat{\mathbf{n}}_i$, $i = 1, 2, 3$ is

$$(\mathbf{A} - \lambda_i\mathbf{I})\hat{\mathbf{n}}_i = 0, \quad (i = 1, 2, 3; \text{no summation}) \quad (3.103)$$

Eigenvalues characterize the physical nature of a tensor. They do not depend on coordinates. For a positive definite symmetric tensor \mathbf{A} , all eigenvalues λ_i are (real and) positive since, using 3-102, we have $\lambda_i = \hat{\mathbf{n}}_i \cdot \mathbf{A}\hat{\mathbf{n}}_i > 0$, $i = 1, 2, 3$. Moreover, the set of eigenvectors of a symmetric tensor \mathbf{A} form a mutually orthogonal basis $\{\hat{\mathbf{n}}_i\}$ [15].

3.1.7 Principal scalar invariants

For the system 3-103 to have solutions $\hat{\mathbf{n}}_i \neq 0$ the determinant of the system must vanish. Thus,

$$\det(\mathbf{A} - \lambda_i\mathbf{I}) = 0 \quad (3.104)$$

where,

$$\det(\mathbf{A} - \lambda_i\mathbf{I}) = -\lambda_i^3 + I_1\lambda_i^2 - I_2\lambda_i + I_3 \quad (3.105)$$

This requires that; a cubic equation in λ is solved, usually written as

$$\lambda_i^3 - I_1 \lambda_i^2 + I_2 \lambda_i - I_3 = 0 \quad (3.106)$$

called the characteristic polynomial (or equation) for \mathbf{A} , the solutions of which are the eigenvalues λ_i , $i = 1, 2, 3$.

Here, $I_i(\mathbf{A})$ $i = 1, 2, 3$, are the so-called principal scalar invariants of \mathbf{A} . In terms of \mathbf{A} and its principal values λ_i , $i = 1, 2, 3$, these are given by

$$I_1(\mathbf{A}) = A_{ii} = \text{tr} \mathbf{A} = \lambda_1 + \lambda_2 + \lambda_3 \quad (3.107)$$

$$I_2(\mathbf{A}) = \frac{1}{2} (A_{ii} A_{jj} - A_{ji} A_{ij}) = \frac{1}{2} [(\text{tr} \mathbf{A})^2 - \text{tr}(\mathbf{A}^2)] = \text{tr} \mathbf{A}^{-1} \det \mathbf{A} \quad (3.108)$$

$$I_3(\mathbf{A}) = \varepsilon_{ijk} A_{ii} A_{2j} A_{3k} = \det \mathbf{A} = \lambda_1 \lambda_2 \lambda_3 \quad (3.109)$$

A repeated application of tensor \mathbf{A} to equation 3-102 yields $\mathbf{A}^\alpha \hat{\mathbf{n}}_i = \lambda_i^\alpha \hat{\mathbf{n}}_i$, $i = 1, 2, 3$, for any positive integer α . Using this relation and 3-106 multiplied by $\hat{\mathbf{n}}_i$, the well-known Cayley-Hamilton equation can be obtained;

$$\mathbf{A}^3 - I_1 \mathbf{A}^2 + I_2 \mathbf{A} - I_3 \mathbf{I} = \mathbf{0} \quad (3.110)$$

It states that every (second-order) tensor \mathbf{A} satisfies its own characteristic equation [15].

3.1.8 Further results in tensor calculus

Because vectors and tensor are defined on linear vector spaces, rules for differentiation are similar to those from elementary calculus. For example, if scalar, vector and tensor fields – say, $a \in R$ and $\mathbf{u}, \mathbf{v} \in V$, and $\mathbf{S}, \mathbf{T} \in Lin$ - depend only on the variable $t \in R$, then

$$\frac{d}{dt} (a\mathbf{v}) = \frac{da}{dt} \mathbf{v} + a \frac{d\mathbf{v}}{dt} \quad (3.111)$$

$$\frac{d}{dt} (\mathbf{u} \cdot \mathbf{v}) = \frac{d\mathbf{u}}{dt} \cdot \mathbf{v} + \mathbf{u} \cdot \frac{d\mathbf{v}}{dt} \quad (3.112)$$

$$\frac{d}{dt}(\mathbf{T} \cdot \mathbf{v}) = \frac{d\mathbf{T}}{dt} \cdot \mathbf{v} + \mathbf{T} \cdot \frac{d\mathbf{v}}{dt} \quad (3.113)$$

$$\frac{d}{dt}(\mathbf{T} \cdot \mathbf{S}) = \frac{d\mathbf{T}}{dt} \cdot \mathbf{S} + \mathbf{T} \cdot \frac{d\mathbf{S}}{dt} \quad (3.114)$$

Similarly, it is useful to record the following identities [14]:

$$\nabla \cdot (\mathbf{u} \otimes \mathbf{v}) = (\nabla \cdot \mathbf{u}) \mathbf{v} + \mathbf{u} \cdot \nabla \mathbf{v} \quad (3.115)$$

$$\nabla \cdot (\mathbf{S} \cdot \mathbf{u}) = (\nabla \cdot \mathbf{S}) \cdot \mathbf{u} + \mathbf{S} : (\nabla \mathbf{u}) \quad (3.116)$$

3.2 Kinematics

Kinematics is defined as the study of motion. However, motion not only includes the current movement of a body, but also how the position of a particle within a particular configuration of a body has changed relative to its position in reference configuration. Here, a body to be a collection of material particles and configuration of the body to be the specification of the positions of each of the particles in the body at a particular time t is defined. Motion can be defined, therefore, as a sequence of configurations parameterized by time [14].

It will prove useful to locate a generic particle in a reference configuration β_0 , at time $t = 0$, via a position vector \mathbf{X} , and likewise the position of the same particle in a current configuration β_t , at time t , via a position vector \mathbf{x} . Although the reference configuration is often taken to be a stress-free, undeformed configuration, it doesn't need to be. It is also useful to refer \mathbf{X} and \mathbf{x} to different coordinate systems (that are related by a known translation and rotation): for Cartesian components, we refer \mathbf{X} and \mathbf{x} to the coordinate systems $\{\mathbf{O}; \mathbf{E}_A\}$ and $\{\mathbf{o}; \mathbf{e}_i\}$, respectively. Hence, the position vectors have representations $\mathbf{X} = X_A \mathbf{E}_A$ and $\mathbf{x} = x_i \mathbf{e}_i$, where summation is implied over dummy indices $A = 1, 2, 3$ and $i = 1, 2, 3$ in E^3 . Without a loss of generality, however, origins \mathbf{O} and \mathbf{o} coincide as seen in Figure 3.2. The displacement vector \mathbf{u} for each material particle is thus given by $\mathbf{u} = \mathbf{x} - \mathbf{X}$. With the exception of a rigid body motion, each particle constituting a body can experience a different displacement.

The position of a material particle, relative to a common origin, is given by \mathbf{X} and \mathbf{x} in these two configurations, respectively. The displacement $\mathbf{u} = \mathbf{x} - \mathbf{X}$ and \mathbf{E}_A and \mathbf{e}_i are orthonormal bases.

There are four basic approaches to describe the kinematics of a continuum: the material, referential, spatial and relative approaches.

In the material approach, motion is described via the particles themselves and time; this approach is not particularly useful in solid mechanics [14].

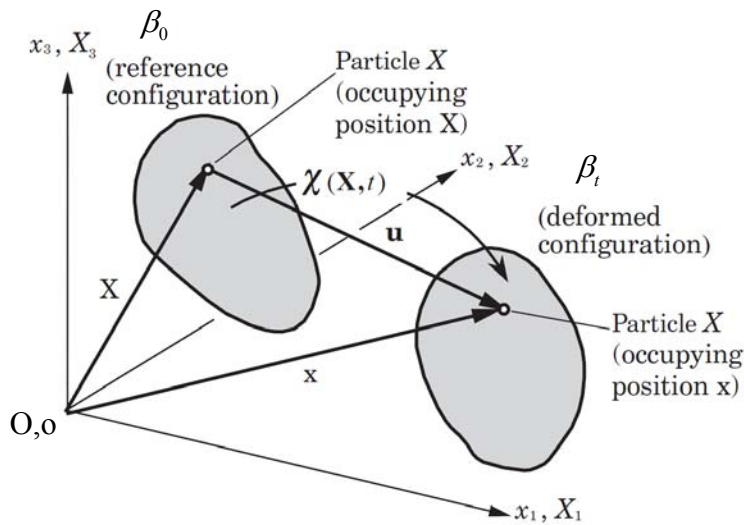


Figure 3.2 : Reference and deformed configurations of a body [16].

The Lagrangian (referential) description is a characterization of the motion with respect to the material coordinates (X_1, X_2, X_3) and time t . In material description attention is paid to a particle, what happens to the particle as it moves is observed. Traditionally, the material description is often referred to as the Lagrangian description. Note that at $t=0$ we have the consistency condition $\mathbf{X} = \mathbf{x}$ and $X_A = x_a$.

The Eulerian (spatial) description is a characterization of the motion with respect to the spatial coordinates (x_1, x_2, x_3) and time t . In spatial description attention is paid to a point in space, and what happens at the point as the time changes is studied.

In fluid mechanics, the Eulerian description in which all relevant quantities referred to the position in space at time t is quite often used. It is not useful to refer the quantities to the material coordinates X_A , $A = 1, 2, 3$, at $t=0$, which are, in general, not known in fluid mechanics. However, in solid mechanics both types of description

is used. Due to the fact that the constitutive behavior of solids is often given in terms of material coordinates the Lagrangian description preferred oftenly.

Finally, in the relative approach one uses independent variables (\mathbf{x}, τ) where τ is a measure of time often related to an intermediate configuration; this approach is useful in viscoelasticity [14, 15].

Let the positions of material particles at time t depend on their original positions, viz.,

$$\mathbf{x} = \mathbf{x}(\mathbf{X}, t), \quad \mathbf{x}, \mathbf{X} \in V \quad t \in R \quad (3.117)$$

Hence the associated displacement field is given by,

$$\mathbf{u}(\mathbf{X}, t) = \mathbf{x}(\mathbf{X}, t) - \mathbf{X} \quad (3.118)$$

When primarily in the motion of individual material particles is interested, it is useful to consider what happens to generic differential line segments as a body passes from one configuration to another. Hence, let $d\mathbf{x}$ be an oriented differential line segment in β_t that was originally $d\mathbf{X}$ in β_0 . A fundamental question then is how do we relate these two differential position vectors? Recall that a second order tensor transforms a vector in to a new vector. Hence in direct and Cartesian component notations, at each time t , let

$$d\mathbf{x} = \mathbf{F} \cdot d\mathbf{X}, \quad dx_i = F_{iA} \cdot dX_A \quad (3.119)$$

Where \mathbf{F} is a second order tensor that accomplishes the desired transformation. The quantify \mathbf{F} is crucial in nonlinear continuum mechanics and is primary measure of deformation, called the deformation gradient. In general \mathbf{F} has nine components for all t , and characterizes the behavior of motion in the neighborhood of a point.

Expression 3-119 clearly defines a linear transformation which generates a vector $d\mathbf{x}$ by the action of the second order tensor \mathbf{F} on the vector $d\mathbf{X}$. Hence, equation 3-119 serves as transformation rule and \mathbf{F} is said to be a two point tensor involving points in two distinct configurations. One index describes spatial coordinates, x_a and the other material coordinates, X_A . In summary: material tangent vectors map (i.e. transform) in to spatial tangent vectors via the deformation gradient [15].

Because \mathbf{x} is a function of \mathbf{X} , at each fixed time t , the chain rule requires

$$\mathbf{dx} = \frac{\partial \mathbf{x}}{\partial \mathbf{X}} \cdot \mathbf{dX} , \quad dx_i = \frac{\partial x_i}{\partial X_A} \cdot dX_A \quad (3.120)$$

Moreover, comparing equations above reveals that

$$\mathbf{F} = \frac{\partial \mathbf{x}}{\partial \mathbf{X}} = F_{iA} \mathbf{e}_i \otimes \mathbf{E}_A , \quad \text{where } F_{iA} = \frac{\partial x_i}{\partial X_A} \quad (3.121)$$

This provides a method for computing the components F given a referential description of the motion relative to a Cartesian coordinate system [14].

Assuming equation 3-117 is invertible, that is X can be written as a function of x at a fixed time t, we can alternatively consider

$$\mathbf{dX} = \frac{\partial \mathbf{X}}{\partial \mathbf{x}} \cdot \mathbf{dx} , \quad dX_A = \frac{\partial X_A}{\partial x_i} dx_i \quad (3.122)$$

With

$$\mathbf{F}^{-1} = \frac{\partial \mathbf{X}}{\partial \mathbf{x}} = F^{-1}_{Ai} \mathbf{E}_A \otimes \mathbf{e}_i , \quad \text{where } F^{-1}_{Ai} = \frac{\partial X_A}{\partial x_i} \quad (3.123)$$

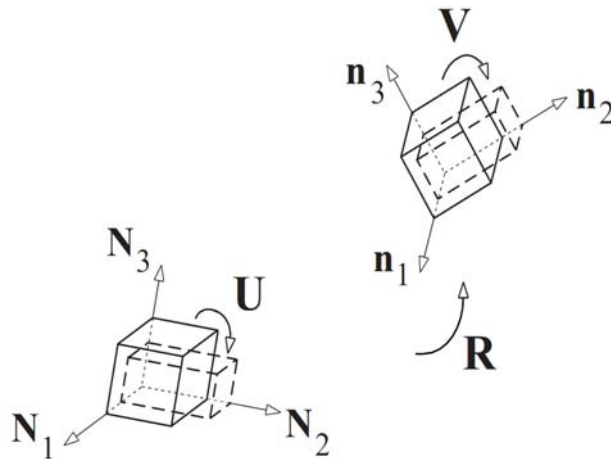


Figure 3.3 : Schematic representation of the polar decomposition of deformation gradient. Material element is first stretched by U and then rotated by R, or first rotated by R and then stretched by V [17].

It is important to observe that position vectors \mathbf{dx} can be mapped from \mathbf{dX} via a rigid body motion (i.e., a translation and/or rotation), a "deformation" (i. e., extension and

shear), or a combination of both. Indeed, it can be shown that \mathbf{F} can be decomposed via

$$\mathbf{F} = \mathbf{R} \cdot \mathbf{U} = \mathbf{V} \cdot \mathbf{R} \quad (3.124)$$

Where $\mathbf{R} \in Orth^+$ (i.e., $\mathbf{R}^{-1} = \mathbf{R}^T$ and $\det \mathbf{R} = 1$) represents the rigid body motion, $\mathbf{U} \in Psym$ (i.e., $\mathbf{U}^T = \mathbf{U}$ and is positive definite) is defined in the reference configuration β_0 , and $\mathbf{V} \in Psym$ is defined in the current configuration β_t . Referred to Cartesian coordinates,

$$\mathbf{R} = R_{iA} \mathbf{e}_i \otimes \mathbf{E}_A = R_{Ai} \mathbf{E}_A \otimes \mathbf{e}_i, \quad \mathbf{U} = U_{AB} \mathbf{E}_A \otimes \mathbf{E}_B, \quad \mathbf{V} = V_{ij} \mathbf{e}_i \otimes \mathbf{e}_j \quad (3.125)$$

Hence, \mathbf{R} is a two-point tensor, whereas \mathbf{U} and \mathbf{V} are one-point tensors. \mathbf{U} and \mathbf{V} represent the complete deformation (extension and shear), but are called right and left "stretch" tensors, respectively, because their principal values are the principal stretches (e.g., current divided by reference lengths) experienced by the body at a point. Equation 3-124 can be interpreted, therefore, as "stretch" followed by a "rigid rotation" ($\mathbf{R} \cdot \mathbf{U}$) or a "rigid rotation" followed by "stretch" ($\mathbf{V} \cdot \mathbf{R}$); it is called the polar decomposition theorem.

At first, the right Cauchy-Green tensor \mathbf{C} defined by

$$\mathbf{C} = \mathbf{F}^T \mathbf{F} \quad (3.126)$$

\mathbf{C} is symmetric and positive definite and, therefore, holds

$$\mathbf{C} = \mathbf{F}^T \mathbf{F} = (\mathbf{F}^T \mathbf{F})^T = \mathbf{C}^T \quad (3.127)$$

Further, we will define

$$\det \mathbf{C} = (\det \mathbf{F})^2 = J^2 > 0 \quad (3.128)$$

with J as the determinant of \mathbf{F} called the volume ratio.

A commonly used strain measurement is the Green-Lagrange strain tensor \mathbf{E} defined by

$$\mathbf{E} = (\mathbf{F}^T \mathbf{F} - \mathbf{I}) = \frac{1}{2}(\mathbf{C} - \mathbf{I}) \quad (3.129)$$

which is based on the observation of the change of squared lengths of line elements. Since \mathbf{C} and \mathbf{I} are symmetric \mathbf{E} is also symmetric. \mathbf{C} and \mathbf{E} are defined on the undeformed reference configuration and are, therefore, referred to as material strain tensors.

An important strain measure in terms of spatial coordinates is the left Cauchy-Green (so called Piola deformation tensor) tensor \mathbf{B} defined by

$$\mathbf{B} = \mathbf{F}\mathbf{F}^T \quad (3.130)$$

The second order tensor \mathbf{B} is as \mathbf{C} symmetric and positive definite

$$\mathbf{B} = \mathbf{F}\mathbf{F}^T = (\mathbf{F}\mathbf{F}^T)^T = \mathbf{B}^T \quad (3.131)$$

\mathbf{B} can be also defined by the the inverse of right Cauchy-Green deformation tensor \mathbf{C} , i.e., $\mathbf{B} = \mathbf{C}^{-1}$, with $\mathbf{C}^{-1} = (\mathbf{F}^T \mathbf{F})^{-1} = \mathbf{F}^{-1} \mathbf{F}^{-T}$.

It can be shown that;

$$\det \mathbf{B} = (\det \mathbf{F})^2 = J^2 > 0 \quad (3.132)$$

holds.

An observation of the change of squared lengths of line elements defined in the current configuration leads to the spatial counterpart of \mathbf{E} , namely the Euler-Almansi strain tensor \mathbf{e} defined by

$$\mathbf{e} = \frac{1}{2}(\mathbf{I} - \mathbf{F}^{-T} \mathbf{F}^{-1}) = \frac{1}{2}(\mathbf{I} - \mathbf{B}^{-1}) \quad (3.133)$$

It can be shown that the right Cauchy-Green tensor \mathbf{C} and left Cauchy-Green tensor \mathbf{B} may be expressed as

$$\mathbf{C} = \mathbf{F}^T \mathbf{F} = \mathbf{U}^T \mathbf{R}^T \mathbf{R} \mathbf{U} = \mathbf{U}^2 \quad (3.134)$$

$$\mathbf{B} = \mathbf{F}\mathbf{F}^T = \mathbf{V}\mathbf{R}\mathbf{R}^T\mathbf{V}^T = \mathbf{V}^2 \quad (3.135)$$

\mathbf{C} and \mathbf{B} are both one-point, symmetric tensors that are independent of rigid body motion, \mathbf{C} being defined in the reference configuration β_0 and \mathbf{B} in the current configuration β_t . When referred to Cartesian coordinates,

$$\mathbf{C} = C_{AB}\mathbf{E}_A \otimes \mathbf{E}_B, \text{ where } C_{AB} = \frac{\partial x_i}{\partial X_A} \frac{\partial x_i}{\partial X_B}, \quad (3.136)$$

$$\mathbf{B} = B_{ij}\mathbf{e}_i \otimes \mathbf{e}_j, \text{ where } B_{ij} = \frac{\partial x_i}{\partial X_A} \frac{\partial x_j}{\partial X_A} \quad (3.137)$$

The **stretch** (extension) **ratios** related to the principal strain components \mathbf{C}_{ii} and \mathbf{E}_{ii} are defined as [50]:

$$\lambda_i = F_{ii} = \frac{\partial x_i}{\partial X_i}, \quad C_{ii} = \lambda_i^2 \text{ and } E_{ii} = \frac{1}{2}(\lambda_i^2 - 1) \quad i = 1, 2, 3 \quad (3.138)$$

3.3 Basic Mechanics of General Soft Tissues

Biological tissues are roughly divided into: hard tissues like bone and tooth, and soft tissues such as skin, muscle, blood vessel, and lung. Hard tissues contain mineral, while soft tissues do not. As a result, soft tissues have very different mechanical properties. One of the major differences in mechanical properties is that soft tissues are much more deformable than hard tissues. Therefore, infinitesimal deformation theories that are applied to metals and hard plastics cannot be used for soft tissues; instead, finite (large) deformation theories that are useful for rubber elasticity are often used to describe the mechanical behavior of soft tissues due to their range of deformation [7].

3.3.1 Inhomogeneous structure

Biological soft tissues are composed mainly of cells and intercellular substances, the latter consisting of connective tissues such as collagen and elastin, and ground substance (hydrophilic gel). These components have different physical and chemical properties, and their contents differ from tissue to tissue and even from location to

location within a tissue. Thus, the mechanical properties depend both on tissue and on location as mentioned in Section 2.

In figure 3.4, stress-strain relations for the canine nuchal ligament, sole tendon, and intestinal smooth muscle, which are rich in collagen, elastin, and smooth muscle (cell), respectively are shown. The elastin-rich nuchal ligament has much less strength and much more flexibility than the collagen-rich sole tendon. The intestinal smooth muscle is much softer than the other two tissues, and its stress-strain curve has a wide hysteresis loop, which indicates that the tissue is viscoelastic. The elastic moduli calculated from the se relations are approximately 0.4, 350, and 0.03 MPa in the nuchal ligament, sole tendon, and intestinal smooth muscle, respectively [7].

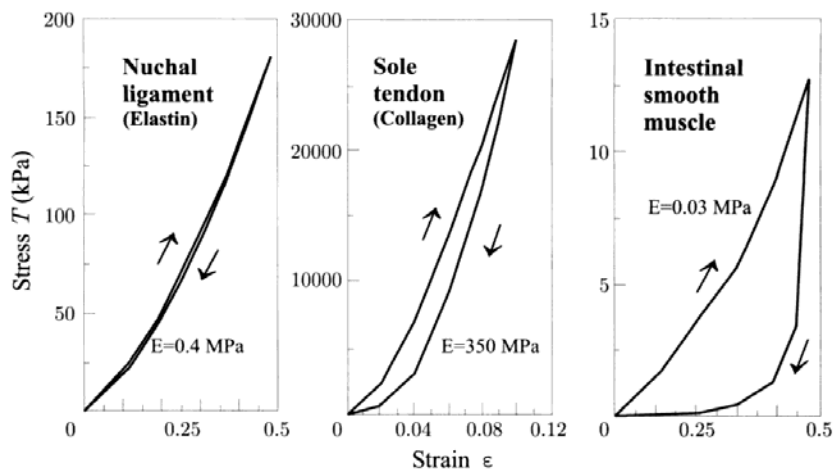


Figure 3.4 : Tensile properties of elastine-rich canine nuchal ligament, collagen-rich sole tendon and intestinal smooth muscle [24].

3.3.2 Nonlinear behavior

The main property of soft tissues may be outlined as being their nonlinear behaviour. Kwan described the phenomenon as follows: "Under uniaxial tension, parallel-fibered collagenous tissues exhibit a non-linear stress-strain relationship characterized by an initial low modulus region, an intermediate region of gradually increasing modulus, a region of maximum modulus which remains relatively constant, and a final region of decreasing modulus before complete tissue rupture occurs. The low modulus region is attributed to the removal of the undulations of collagen fibrils that normally exist in a relaxed tissue [51]. As the fibrils start to resist the tensile load, the modulus of the tissue increases. When all the fibrils become taut and loaded, the tissue modulus reaches a maximum value, and thereafter, the tensile stress increases linearly with

increasing strain. With further loading, groups of fibrils begin to fail, causing the decrease in modulus until complete tissue rupture occurs." A typical tensile test curve is shown in Fig. 3.5a. From a functional point of view, the first parts of the curve are more useful since they correspond to the physiological range in which the tissue normally functions [18].

Also, Holzapfel emphasizes the intermolecular cross links of collagen gives the connective tissues the strength which varies with age, pathology, etc. Table 3.1 shows the correlation between the collagen content in the tissue, % dry weight, and its ultimate tensile strength [22].

Table 3.1: Mechanical properties [19], [5], [20] and associated biochemical data [21] of some representative organs mainly consisting of soft connective tissues

Material	Ultimate Tensile Strength [MPa]	Ultimate Tensile Strain [MPa]	Collagen (% dry weight)	Elastin (% dry weight)
Tendon	50-100	10-15	75-85	< 3
Ligament	50-100	10-15	70-80	10-15
Aorta	0.3-0.8	50-100	25-35	40-50
Skin	1-20	30-70	60-80	5-10
Articular Cartilage	9-40	60-120	40-70	-

3.3.3 Viscoelasticity

The experimental results shown in Figure 3.5a reveals the relationship between stress and strain in the static case. However, when the equilibrium is not reached, a history-dependent component exists in the mechanical behavior of living tissues. When measured in dynamic extension, the stress values appear higher than those at equilibrium, for the same strain. The resulting tensile curve appears steeper than the one at equilibrium (Fig. 3.5a). When a tissue is suddenly extended and maintained at its new length, the stress gradually decreases slowly against time. This phenomenon is called stress relaxation (Fig 3.6a). When the tissue is suddenly submitted to a constant tension, its lengthening velocity decreases against time until equilibrium. This phenomenon is called creep (Fig. 3.6b). Under cyclic loading, the stress-strain curve shows two distinct paths corresponding to the loading and unloading trajectories. This phenomenon is named hysteresis (Fig. 3.6c). As a global statement, the stress at any

instant of time depends not only on the strain at that time, but also on the history of the deformation. These mechanical properties, observed for all living tissues, are common features of viscoelasticity [5].

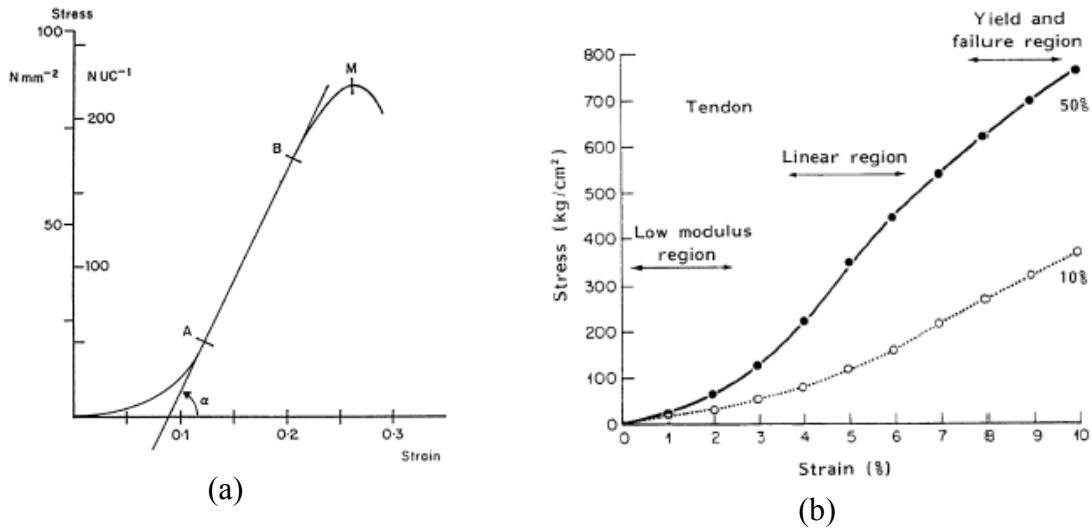


Figure 3.5 : Load-extension curve of a tendon (a), Influence of the strain rate [45, 46].

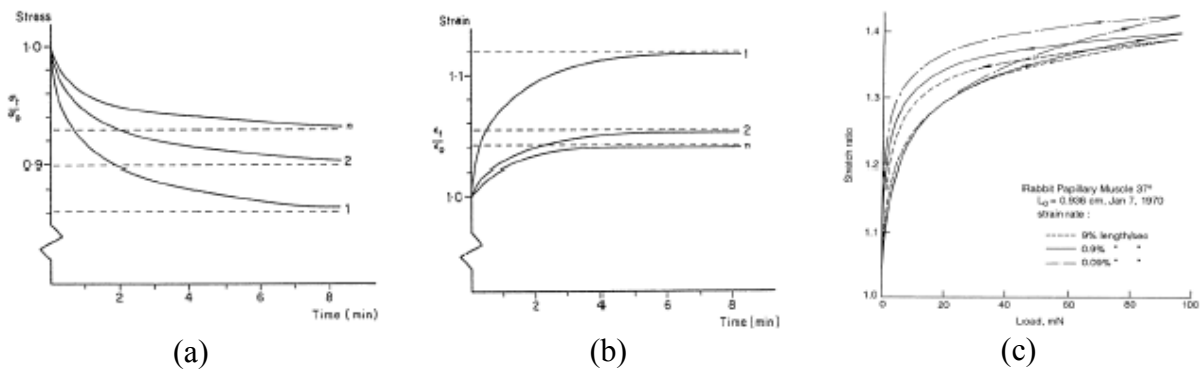


Figure 3.6 : Viscoelastic behavior: a) stress relaxation , b) creep, c) hysteresis [46, 47].

3.3.4 Anisotropy

Since collagen and elastin are long-chained high polymers, they are intrinsically anisotropic. Moreover, not only their fibers but also cells are oriented in tissues and organs in order that they function most effectively. Inevitably, almost all biological tissues are mechanically anisotropic. For example, skin has very different properties in two orthogonal directions; see Figure 3.7 [25] and [26]; it cannot deform much in the direction of Langer's line [27], but can deform much more in the perpendicular direction. Collagen fibers in the articular cartilage are preferentially oriented to the

split line and, therefore, this tissue also shows anisotropic behavior; see Figure 3.8 [28].

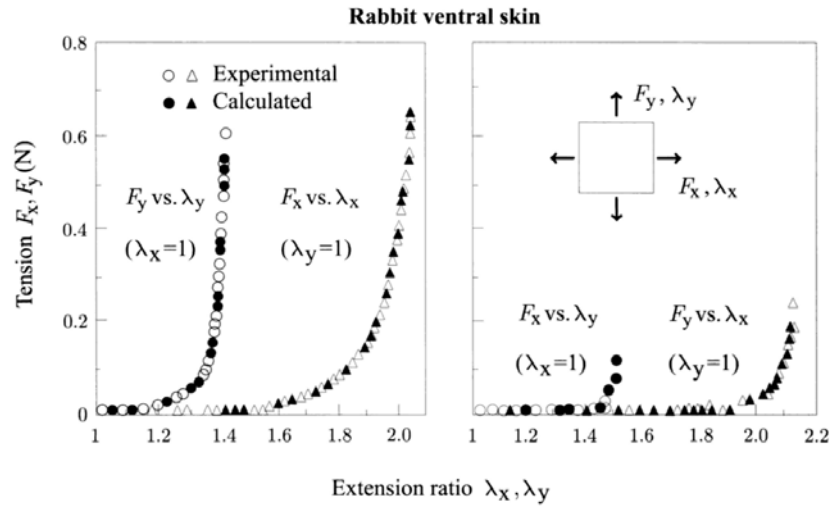


Figure 3.7 : Tension-extension ratio relations of rabbit skin [49].

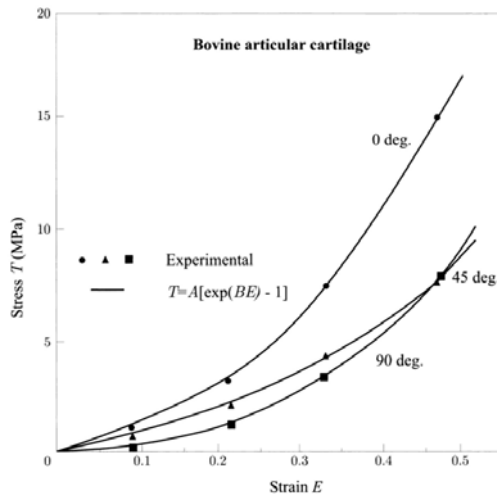


Figure 3.8 : Tensile properties of articular cartilage.

3.3.5 Strain rate insensitivity

Because of the viscoelastic characteristics of soft materials, they show different properties under different strain rates (test speed). In fact, higher strain rates give higher stresses; see Figure 3.9 [30]. However, such a strain rate effect is not very large in biological soft tissues; there are not very large differences in the stress-extension ratio curves across three orders of magnitude of the tensile speed (CT in Figure 3.9). In addition, the area of the hysteresis loop (H in Figure 3.9) does not

depend upon strain rate. Generally speaking, therefore, biological soft tissues are mechanically not very sensitive to strain rate [7].

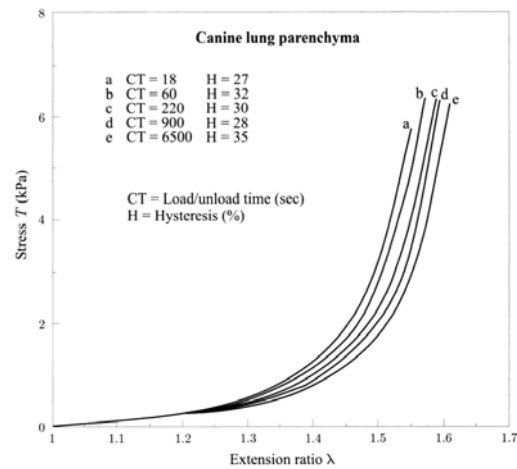


Figure 3.9 : Tensile properties of lung parenchyma at different strain rates [48].

3.3.6 Incompressibility

Most biological soft tissues have a water content of more than 70%. Therefore, they hardly change their volume (isovolumic) even if load is applied, and they are almost incompressible. The incompressibility assumption is applicable to most biological soft tissues; it has been confirmed experimentally in arterial wall [31] and [29]. However, it is not the case in the articular cartilage, because the tissue is micro-porous and, therefore, water can enter and leave pores depending upon load [28]. The incompressibility assumption is very important in the formulation of constitutive laws for soft tissues because the sum of all principal (logarithmic) strains is always zero [7].

3.4 Mechanical Behaviour of Arterial Wall

Each constitutive framework and its associated set of material parameters require detailed studies of the particular material of interest. Its reliability is strongly related to the quality and completeness of available experimental data, which may come from appropriate in vivo tests or from in vitro tests that mimic real loading conditions in a physiological environment. In vivo tests seem to be preferable because the vessel is observed under real life conditions. However, in vivo tests have major limitations because of, for example, the influence of hormones and neural control. Moreover, data sets from the complex material response of arterial walls subject to simultaneous

cyclic inflation, axial extension and twist can only be measured in an in vitro experiment. Only with such data sets can the anisotropic mechanical behavior of arterial walls be described completely. In addition, in in vitro experiments the contraction state (active or passive) of the muscular media has to be determined.

The presence of a residual stress field can have a major impact on a body's effective mechanical properties [35]. Evidence of the existence of residual stresses in the arterial wall at the unloaded state is given in Fung [61]. With a longitudinal cut along the vessel wall the unloaded specimen springs open and its cross section becomes a sector. The opening angle of the vessel wall is time-dependent after the sudden relief of the initial residual stress. It shows that the artery is not stress-free at the unloaded state [54, 57].

The most commonly used method for describing residual stress in artery wall was proposed by Chuong and Fung [62]. The method builds on the experimental observation that an artery ring opens up to a cylindrical sector, which is approximately stress free, after a radial cut is applied to the wall. If the open sector geometry and the constitutive equation for the material are known, the residual stress in the intact (i.e., closed and unloaded) configuration can be determined from the boundary value problem (BVP) that governs the closing motion.

Zhou states the cut experiment remains perhaps the most reliable method for studying residual stress. If one assumes that both the intact configuration and the open sector are perfectly cylindrical, and that the closing motion involves pure bending, the residual strains in the intact state can be derived as a function of the open sector geometry (the opening angle and radii) [54].

In the scope of this study mechanical behaviour consideration is only limited to residual strains on arterial wall.

3.4.1 Residual strains and stresses

Residual strains and stresses are those that exist in a body when all external loads are removed. Because residual stresses can significantly affect the mechanical behaviour of a component the measurement of these stresses is and the prediction of their effect on mechanical behaviour are important objectives in many engineering problems like constitutive formulations and stress analysis [33, 35, 36].

Residual stresses are present in a variety of biological tissues and organs, and can have a significant impact on mechanical response to external loading (see [34] for example) Some of the earliest work on residual stresses in soft biological tissues were studies of arteries.

Recent reports also suggest that residual stress and strains might even be the key to understanding stress-modulated remodeling of the artery under disease conditions like atherosclerosis and hypertension [14, 38]. Given their relative significance in vascular mechanics, it is important to ensure that the experiments performed to determine residual strains and the assumptions made during the analysis are appropriate [37].

3.4.1.1 Opening angle

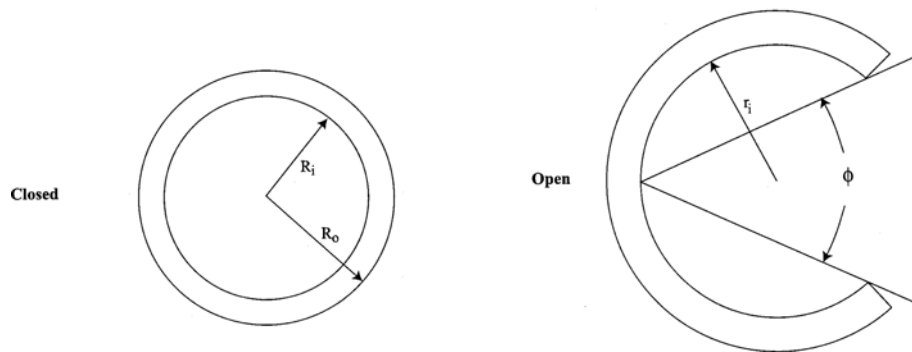


Figure 3.10 : Schematic of the opening angle experiment which is used for assessing the residual strain in biological organs with approximately cylindrical geometry. [39]

The opening angle experiment is performed by making a radial cut in a ring of tissue and then measuring the resulting opening angle ϕ . A schematic representation of this experiment is shown in Figure 3.10. In this study, the configuration of the ring after it has been excised from the organ is referred, but before the radial cut, as the closed configuration. The configuration taken by the ring after the radial cut has been made will be referred to as the open configuration.

It is typically assumed that the geometry of the closed configuration and the constitutive equation for the stress-free material are given. The geometry of the closed configuration is specified by the inner and outer radii, R_i and R_o , respectively. The material composing the ring is assumed to be incompressible and

hyperelastic. Generally, the material is taken to be uniform, even if this condition is not essential. Motivated by the cylindrical symmetry of the geometry, it is assumed to be a function of the radial position only, and to have no shear components [39].

3.4.1.2 Kinematics of the stress-relieving cut

Consider a material particle located at (R, Θ, Z) , in the central region of a radially cut arterial segment, that is mapped to (ρ, ϑ, ξ) in the central region of an associated unloaded intact configuration according to [14];

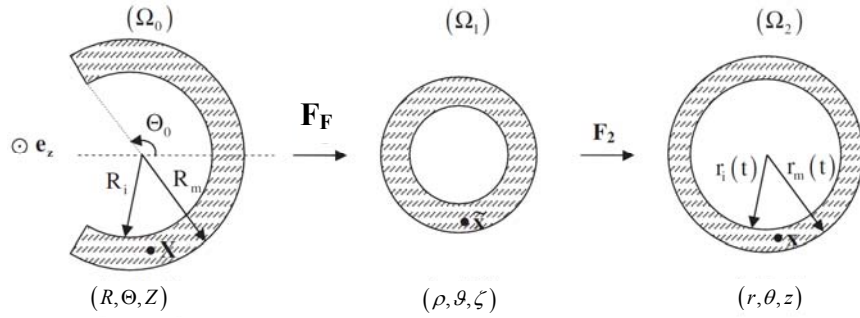


Figure 3.11 : Kinematics of the arterial wall relative various configurations

Nearly stress-free reference configuration (Ω_0) , the excised, unloaded configuration (Ω_1) , and the in vivo loaded configurations (Ω_2) having coordinates (R, Θ, Z) , (ρ, ϑ, ζ) , (r, θ, z) , is showed respectively [52].

$$\rho = \rho(R) \quad \vartheta = \frac{\pi}{\Theta_0} \Theta \quad \zeta = \Lambda Z \quad (3.139)$$

Where Θ_0 is one of the aforementioned angles and $\Lambda = \Lambda_\zeta$ is an axial stretch ratio associated with the residual stress. Therefore, in the absence of the residual stress $\Theta_0 = \pi$ and $\Lambda = 1$.

According to these values, the physical components of deformation gradient tensor in cylindrical coordinates associated with the mapping in equation 3.139 are

$$[\mathbf{F}_F] = \begin{bmatrix} \frac{\partial \rho}{\partial R} & \frac{\partial \rho}{R \partial \Theta} & \frac{\partial \rho}{\partial Z} \\ \frac{\partial \mathcal{G}}{\partial R} & \frac{\rho \partial \mathcal{G}}{R \partial \Theta} & \frac{\rho \partial \mathcal{G}}{\partial Z} \\ \frac{\partial \zeta}{\partial R} & \frac{\partial \zeta}{R \partial \Theta} & \frac{\partial \zeta}{\partial Z} \end{bmatrix} = \begin{bmatrix} \frac{\partial \rho}{\partial R} & 0 & 0 \\ 0 & \frac{\pi \rho}{\Theta_0 R} & 0 \\ 0 & 0 & \Lambda \end{bmatrix} \quad (3.140)$$

Applying the incompressibility constraint $\det \mathbf{F}_F = 1$, yields

$$\frac{\partial \rho}{\partial R} \left(\frac{r \pi}{R \Theta_0} \right) \Lambda = 1, \quad \rho \frac{\partial \rho}{\partial R} = \frac{\Theta_0 R}{\pi \Lambda} \quad (3.141)$$

and integrating this relation with respect to R to yield,

$$\rho^2 - \rho_i^2 = \frac{\Theta_0}{\pi \Lambda} (R^2 - R_i^2), \quad R \in [R_i, R_o] \quad (3.142)$$

Where the “i” and “o” are subscriptions which denote the inside and outside surfaces. This relation allows determining the location of every point in the wall in either configuration given the corresponding location in other configuration and knowledge of either the inner or outer radius.

Then, the physical components of the various measures of deformation can be easily determined. The right Cauchy-Green tensor;

$$[\mathbf{C}_F] = [\mathbf{F}_F]^T [\mathbf{F}_F] = \begin{bmatrix} \left(\frac{\Theta_0 R}{\pi \Lambda \rho} \right)^2 & 0 & 0 \\ 0 & \left(\frac{\pi \rho}{\Theta_0 R} \right)^2 & 0 \\ 0 & 0 & \Lambda^2 \end{bmatrix} \quad (3.143)$$

and the Green strain tensor,

$$[\mathbf{E}_F] = \frac{1}{2}(\mathbf{C}_F - \mathbf{I}) = \frac{1}{2} \begin{bmatrix} \left(\frac{\Theta_0 R}{\pi \Lambda \rho}\right)^2 - 1 & 0 & 0 \\ 0 & \left(\frac{\pi \rho}{\Theta_0 R}\right)^2 - 1 & 0 \\ 0 & 0 & \Lambda^2 - 1 \end{bmatrix} \quad (3.144)$$

The residual stress related to the deformation gradient \mathbf{F}_F contains only diagonal terms; thus, components of the associated right stretch tensor \mathbf{U}_F are numerically same as those of \mathbf{F}_F which means \mathbf{F}_F does not contain rigid body motion. ($\mathbf{F} = \mathbf{R}\mathbf{U} = \mathbf{V}\mathbf{R}$).

Residual strain in a typical cylindrical specimen that is not subjected to any inflation, extension or torsion is derived.

In following section residual strain formulations of a cylindrical specimen for reverse deformation will be derived without subjecting any inflation, torsion or extension.. This time, a material particle located at (ρ, ϑ, ξ) , in the central region of an associated unloaded intact configuration, that is mapped to (R, Θ, Z) in the central region of a radially cut arterial segment is considered.

3.4.1.3 Reverse formulation

Mapping for reverse formulation of the opening angle method may be stated as follows; [59] Subscript ‘‘R’’ stands for reverse formulation and correspond to the deformation \mathbf{F}_2 shown in figure 3.14.

$$(\rho, \vartheta, \zeta) \rightarrow (R, \Theta, Z) \quad (3.145)$$

$$R = R(\rho), \quad \Theta = \frac{(\pi - \Phi_0)}{\pi} \vartheta, \quad Z = \frac{\zeta}{\Lambda} \quad (3.146)$$

In figure 3.14 three different configurations are shown: In vivo configuration, β_1 , which is taken as a reference β_0 for the kinematics, a traction-free excised configuration, β_1 , and a radially-cut, nearly stress-free configuration β_2 . The

deformation gradients are denoted by \mathbf{F}_i and Φ_0 is the opening angle in β_2 . Adopted from [40].

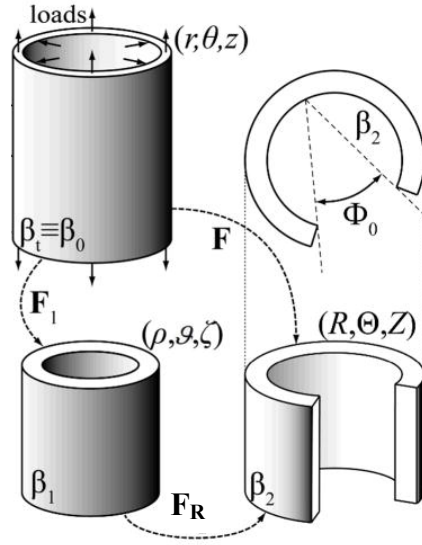


Figure 3.12 : Schema of the different configurations

Hence deformation gradient for this motion is, $\Theta_0 = \pi$;

$$[\mathbf{F}_R] = \begin{bmatrix} \frac{\partial R}{\partial \rho} & \frac{\partial R}{\rho \partial \vartheta} & \frac{\partial R}{\partial \zeta} \\ \frac{\partial \Theta}{\partial \rho} & \frac{R \partial \Theta}{\rho \partial \vartheta} & \frac{R \partial \Theta}{\partial \zeta} \\ \frac{\partial Z}{\partial \rho} & \frac{\partial Z}{\rho \partial \vartheta} & \frac{\partial Z}{\partial \zeta} \end{bmatrix} = \begin{bmatrix} \frac{\partial R}{\partial \rho} & 0 & 0 \\ 0 & \frac{(\pi - \Phi_0)R}{\pi \rho} & 0 \\ 0 & 0 & \frac{1}{\Lambda} \end{bmatrix} \quad (3.147)$$

The right Cauchy-Green tensor can be derived as;

$$[\mathbf{C}_R] = [\mathbf{F}_R]^T [\mathbf{F}_R] = \begin{bmatrix} \left(\frac{\rho \pi \Lambda}{R(\pi - \Phi_0)} \right)^2 & 0 & 0 \\ 0 & \left(\frac{(\pi - \Phi_0)R}{\pi \rho} \right)^2 & 0 \\ 0 & 0 & \left(\frac{1}{\Lambda} \right)^2 \end{bmatrix} \quad (3.148)$$

when Lagrangian strain tensor is calculated using right Cauchy-Green tensor derived above;

$$[\mathbf{E}_R] = \frac{1}{2}(\mathbf{C}_R - \mathbf{I}) = \frac{1}{2} \begin{bmatrix} \left(\frac{\rho\pi\Lambda}{R(\pi - \Phi_0)} \right)^2 - 1 & 0 & 0 \\ 0 & \left(\frac{(\pi - \Phi_0)R}{\pi\rho} \right)^2 - 1 & 0 \\ 0 & 0 & \left(\frac{1}{\Lambda} \right)^2 - 1 \end{bmatrix} \quad (3.149)$$

And strain components can be rearranged by using 3.149;

$$E_{RR} = \frac{1}{2} \left[\left(\frac{\rho\pi\Lambda}{R(\pi - \Phi_0)} \right)^2 - 1 \right],$$

$$E_{\Theta\Theta} = \frac{1}{2} \left[\left(\frac{(\pi - \Phi_0)R}{\pi\rho} \right)^2 - 1 \right], \quad (3.150)$$

$$E_{ZZ} = \frac{1}{2} \left[\left(\frac{1}{\Lambda} \right)^2 - 1 \right]$$

Finally the stretches will be for reverse formulation:

$$\lambda_R = \left(\frac{\rho\pi\Lambda}{R(\pi - \Phi_0)} \right), \quad \lambda_{\Theta} = \left(\frac{(\pi - \Phi_0)R}{\pi\rho} \right), \quad \lambda_Z = \left(\frac{1}{\Lambda} \right) \quad (3.151)$$

As Humprey stated; one can think of these reverse deformation gradients as the inverses of the usual tensors referred to stress-free configuration [14].

4 EXPERIMENTAL STUDIES

4.1 Digital Image Correlation

Data extraction by image analysis is one of the most dynamic areas in non-contacting measurement system development. Digital image correlation (DIC), which is a specific area in this field, has seen impressive growth in the past two decades. In recent years, the digital image correlation method has been modified and extended to encompass a breathtaking number of novel measurement systems. Nowadays, the technology is being used for measuring

- 3-D surface shape and deformations using a variety of illumination sources for a wide range of material systems, with size scales ranging from tens of meters to the microns,
- 2-D surface deformations at the scale of nanometres by using atomic force microscopy and scanning electron microscopy ,
- Interior deformation measurements through volumetric imaging of biological and porous materials using technology such as computer aided tomography, and magnetic resonance imaging,
- Dynamic/impact behaviour of materials using high-speed camera systems.

4.1.1 Background of DIC

The term “digital image correlation” refer to the class of non-contacting measurement methods which includes acquire images of an object, store images digitally and then perform image analysis to get full-field shape, deformation and/or motion measurements. Digital image registration (i.e. matching) has been performed with many types of object-based patterns, including lines, grids, dots and random arrays. Commonly used approaches employ random patterns and comparing sub-regions throughout the image to obtain a full-field of measurements [41].

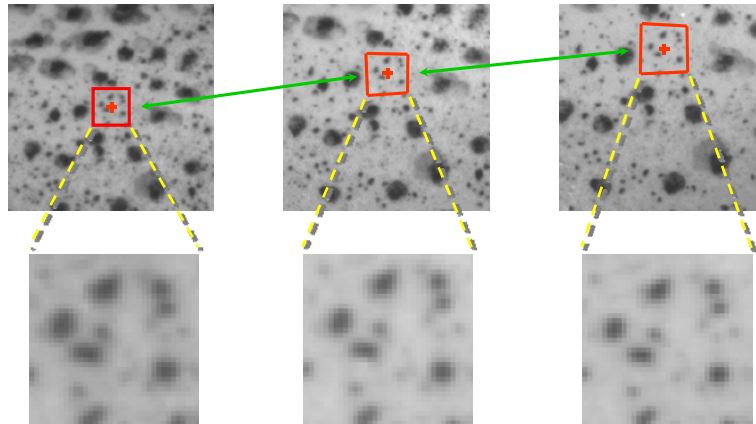


Figure 4.1 : Random pattern in an image [42].

4.1.1.1 Two dimensional (2D) DIC

One of the earliest work to propose the use of computer-based image acquisition and deformation measurements in material systems was by Peters and Ranson in 1981 [43]. Peters and Ranson used the fact that changes in images can be described by the same continuum concepts that govern the deformation of small areas on a surface, an approach was proposed to relate measurable image deformations to object deformations. These original concepts have been refined and incorporated into numerical algorithms to extract object deformations from an image sequence for use in the field of experimental mechanics. The resulting algorithms and software have been used successfully to obtain surface deformations in a various applications.

For image-correlation-based measurement purposes, modern scientific-grade digital cameras are generally used to

- obtain high-quality images on the sensor plane,
- execute onboard digitization of the intensity at each sensor location,
- transfer the digital data to a storage location.

Sutton states that image analysis software can be used to get surface deformations with an accuracy of ± 0.01 pixels or better for in-plane displacement components and point-to-point accuracy of $\pm 100 \mu\epsilon$ for the in-plane surface strains ϵ_{xx} , ϵ_{yy} , and ϵ_{xy} which is tested by many experiments [44].

4.1.1.2 Three dimensional (3D) DIC

Stereo-vision principles developed for robotics, photogrammetry, and other shape and motion measurement applications were modified and successfully implemented to develop and apply a two-camera stereo vision system to accurately measure the full three-dimensional shape and deformation of a curved or planar object, even when the object is subjected to large out-of-plane rotation and displacement. Image analysis software for stereo vision can be used to

- (a) calibrate the camera system,
- (b) perform experiments and simultaneously acquire stereo image pairs, and
- (c) analyze several sets of stereo image pairs to obtain surface deformations.

Sutton suggests that results from various experiments indicate an accuracy of ± 0.015 pixels or better for cross camera image correlation to identify the same image point and point-to-point accuracy of $\pm 100 \mu\epsilon$ for the in-plane surface strains ϵ_{xx} , ϵ_{yy} , and ϵ_{xy} . This accuracy is achievable even when the object is subjected to large rigid-body rotations and arbitrary amounts of rigid-body translations since these motions do not prevent the strain measurements [44].

4.1.2 Essential concepts

Two key assumptions are generally used to convert images into experimental measurements of object shape, displacements, and strains.

Firstly, it is assumed that there is a direct correspondence between the motions of points in the image and motions of points on the object. Since an object is generally approximated as a continuous medium, the correspondence between image and object points ensures that continuum concepts are applicable to describe the relationship between points in an image subset as the object deforms.

Secondly, it is assumed that each subregion has adequate contrast (spatial variation in light intensity) so that accurate matching can be performed to define local image motions. Together with the first assumption, accurate matching can be improved by allowing each image subregion to deform using an appropriate functional form (e.g., affine, quadratic) and hence increase accuracy in the measured motions. The required variation in contrast can be obtained by applying a high-contrast random pattern (e.g.,

painting, adhering, surface machining) as well as it may occur due to the natural surface properties of the material.

4.1.3 Intensity interpolation

To obtain surface deformations from digital images, subregions of digital images are compared. Defining one of the images to be the reference image (i. e., the image of the object when it is considered to be in the undeformed or initial configuration), general deformations of the object will introduce noninteger displacements of the corresponding positions in the reference image. Thus, accurate subpixel estimates for local object motions require that intensity values at integer positions in the reference image are registered with intensity values in the deformed images at noninteger positions. To obtain noninteger estimates for intensity values, the discrete intensity pattern recorded for each deformed image is converted into a continuous functional representation.

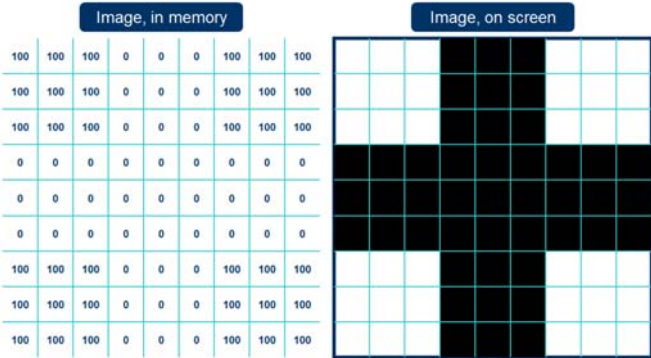


Figure 4.2 : Image in memory and image on screen respectively at initial time.

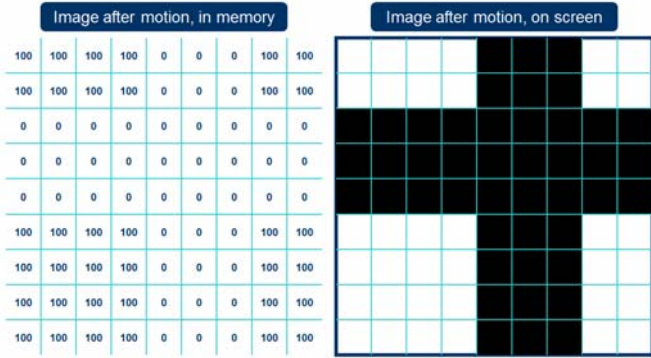


Figure 4.3 : Image in memory and image on screen respectively after motion.

4.1.4 Subset based image displacements and pattern development

Image-plane deformations are extracted through image comparison, where it is common to select an image of the object and designate it to be the *reference* image. All additional images are specified as *deformed* images. Image correlation is performed by comparing small subsets from the digitized textured pattern in the reference image to subsets from each of the deformed images.

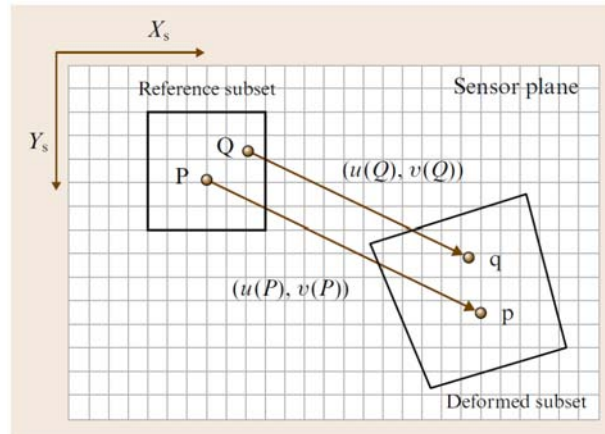


Figure 4.4 : Mapping of sensor positions P and Q in reference subset to p and q in deformed subset [44].

To achieve a usable random pattern of the required size, several approaches have been developed. In each case, the surface must be properly prepared so that the pattern will deform/move with the material system being studied. This process may include degreasing, etching, polishing, and coating of the specimen surface.

4.1.5 3D Digital image correlation

Single-camera 2-D DIC systems are limited to planar specimens that experience little or no out-of-plane motion. Both of these limitations can be overcome by the use of two (or more) cameras observing the surface from different directions. Figure 4.5 (b) shows schematically a two-camera stereo-vision arrangement. The remainder of the developments for stereo-vision systems will focus on a generic two-camera system, though the concepts can be generalized readily to multicamera systems. Three-dimensional image correlation is based on a simple binocular vision principle. Once the cameras are calibrated, the sensor plane locations in the two views for the same object point can be used to determine an accurate estimate for the three-dimensional position of the object location.

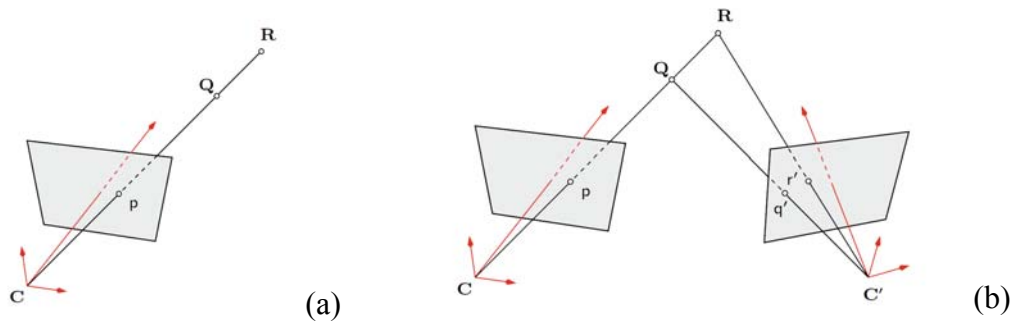


Figure 4.5 : Single camera system (a) vs. two camera system (b) for recovering third dimension.

4.2 3D DIC System Verification Tests

As stated at the beginning, the aim of this study is the direct measurement of strains in and out of arterial wall by using optical correlation methods. Indirect stretches and strains, based on bending assumption, will be also calculated and afterwards results will be compared and evaluated.

Before starting tests on ovine and porcine arterial walls, some experiments are carried on to verify the accuracy of digital image correlation systems on different experimental conditions.

4.2.1 Verification test on mirrored-vision

To measure the strain values in and out of the arterial walls, a test setup which basically involves two quasi-static cameras for gathering 3D displacement - deformation field and a plane mirror will be used. Placing the specimen, speckled on the both sides, in front of the mirror, not only the front side but also the backside will be analyzed by digital image correlation by using the reflection of backside on the mirror. (Figure 4.6)

Specimen used in this experiment is a rubber band speckled on both sides. After stereo calibration, specimen is subjected to pure axial loading.

It is expected to have a successful correlation on both sides and obtaining the same strain values on both sides of the band.

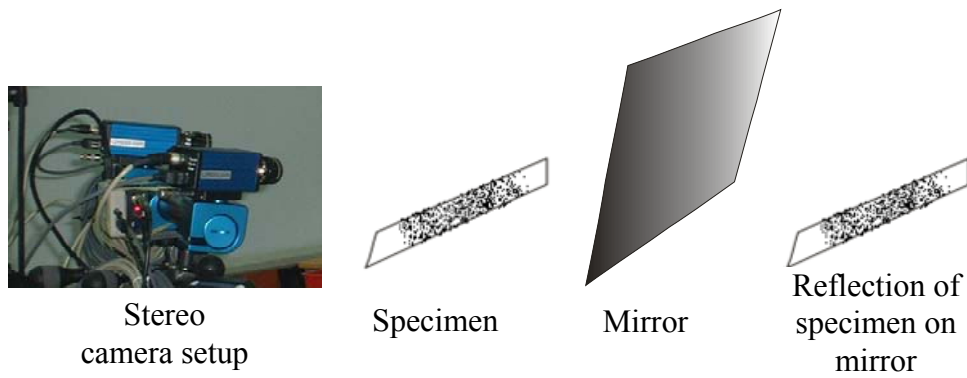


Figure 4.6 : Setup for verification test on mirrored-vision.

On Figure 4.7 (a,b,c,d) shots from process flow of DIC is given by using Vic-3D (Correlated Solutions, USA). Respectively; (a) is the raw image captured by one of the cameras, (b) area of interest is selected to measure deformation and displacement field, (c) a shot from correlation results (Z – displacement [mm]), (d) graphical representation of extracted values (E_{xx})

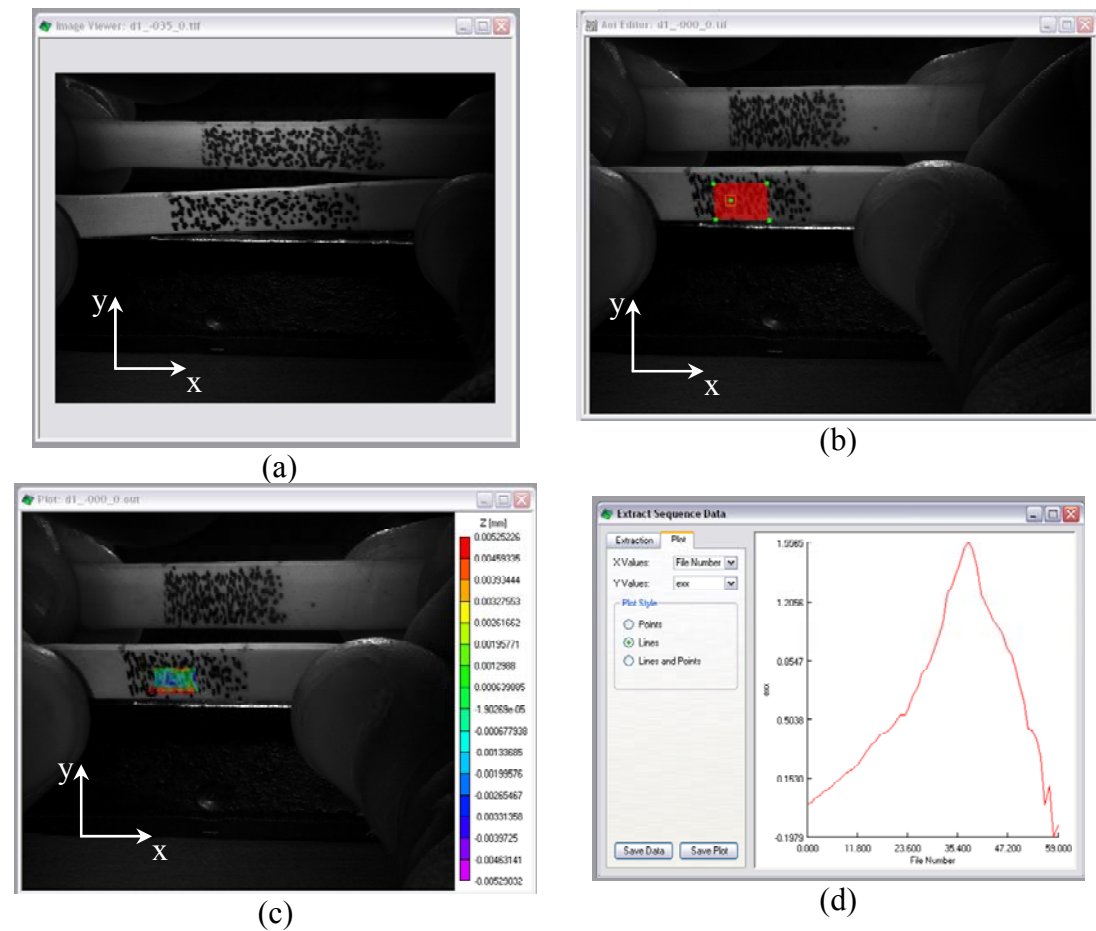


Figure 4.7 : Shots from Vic-3D workspace while mirror correlation test

After calculating displacements and strains for area of interest on both sides of the rubber band, these values are extracted to be compared. Strain equality on both sides is predicted. In the below figures this equality, which comply with the expectations, for strain components, (a) E_{xx} results, (b) E_{yy} results, can be seen. Mean E_{xx} error on this experiment is approximately 0.1% and mean E_{yy} error is 1% for this experiment.

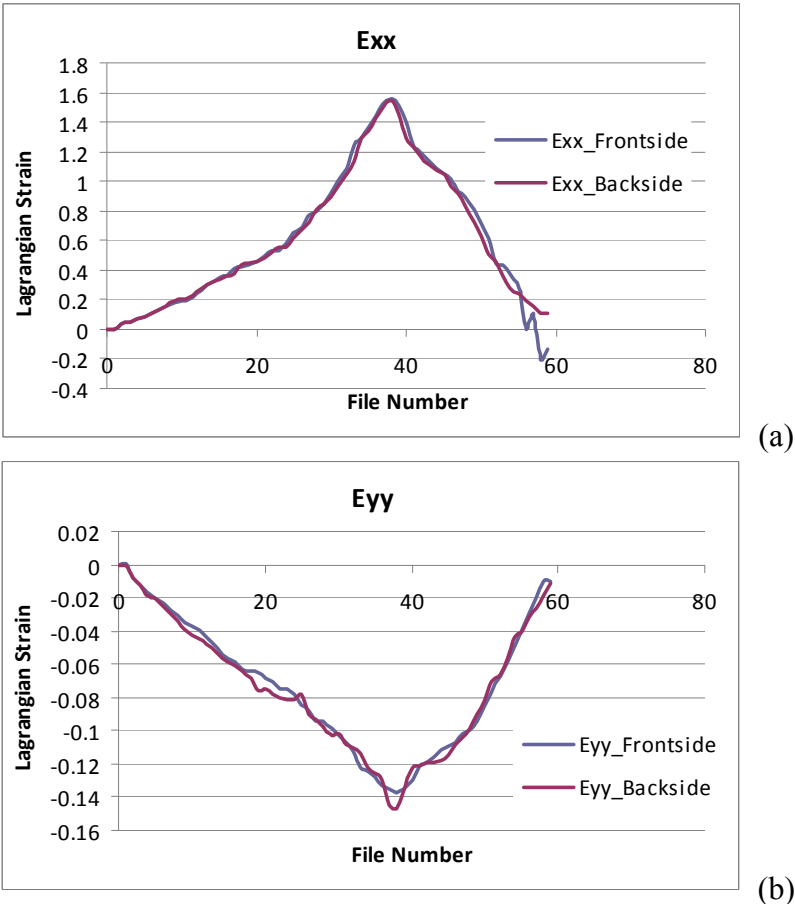


Figure 4.8 : Strain results for verification test on mirrored-vision.

With respect to obtained error values, concept of using a mirror and analyzing on the reflection of specimen is seen to have enough accuracy based on the purpose it is interest to use.

4.2.2 Silicone bar and mechanical extensometer test

Experiencing the needed accuracy on both camera side and the mirror side of the specimen as discussed in Section 4.2.1, as a second step optical results are compared with mechanical measurement devices.

On this sub-experiment, in addition to the previous experiment, the aim is to obtain the accuracy of optical measurement systems and compare the results with conventional measurement systems. In this test a silicon bar specimen with a rectangular cross-section is used. Silicone bar specimen is speckled on both sides and a mechanical extensometer (MTS Model No: 634.31F-25) is attached to the specimen to measure the elongation and strain. Elongation and strain is also followed via the displacement transducer of the head of the universal test machine (MTS 858 Mini Bionix II, Eden Prairie, MN USA).

Test scenario for this test is set to be applying cyclic loading between 0-10mm under displacement control at a rate of 1mm/sec and the same scenario is applied on several specimens.

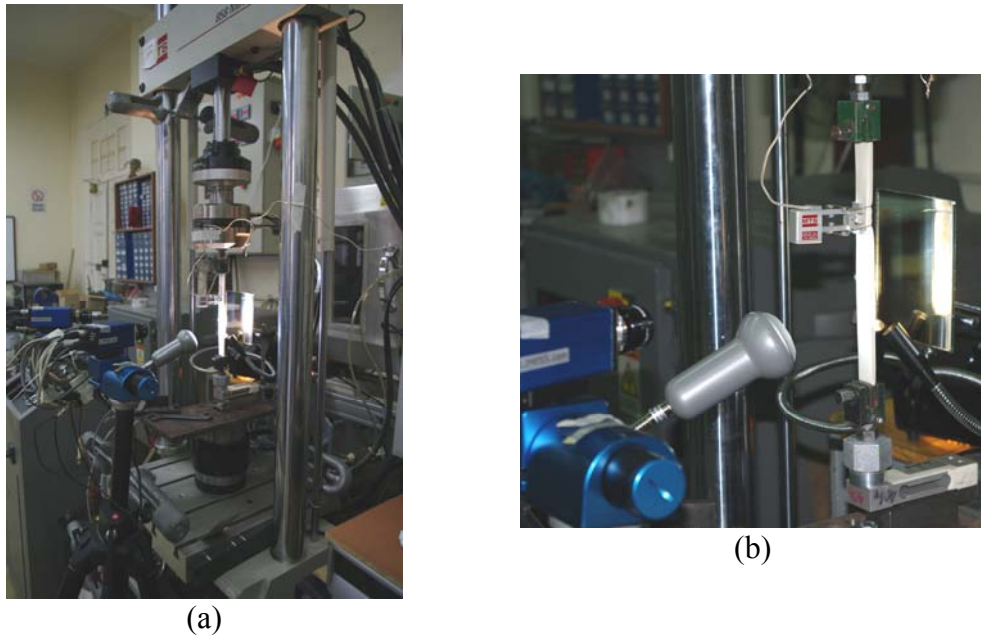


Figure 4.9 : Setup for silicone bar and extensometer test; (a) General view for experimental setup. (b) Close view on specimen, mirror and mechanical extensometer.

On Figure 4.10 (a) displacement results for the head of the universal testing machine, (b) strain results for mechanical measurement systems and (c) strain results for both sides of the silicon bar is given. Since mechanical systems in this setup can only measure displacements in one direction, only E_{yy} component of strain is compared.

Error values for between different comparison groups has been figured out as follows in Table 4.1:

Table 4.1: Error values for silicone bar and mechanical extansometer test.

Error between	Error %
MTS Head and MTS Extansometer	0.7
Frontside and backside of silicone bar	0.7
Mean optical values to mean MTS values	2

Displacement results for the head of test machine (a), strain results (E_{yy}) for mechanical measurement systems (b) and strain results (E_{yy}) for both sides of the silicon bar (c) is shown in Figure 4.10. When optical correlation systems are compared to conventional mechanical measurement systems depending of the error values above ,, optical measurement systems are seen to have enough accuracy.

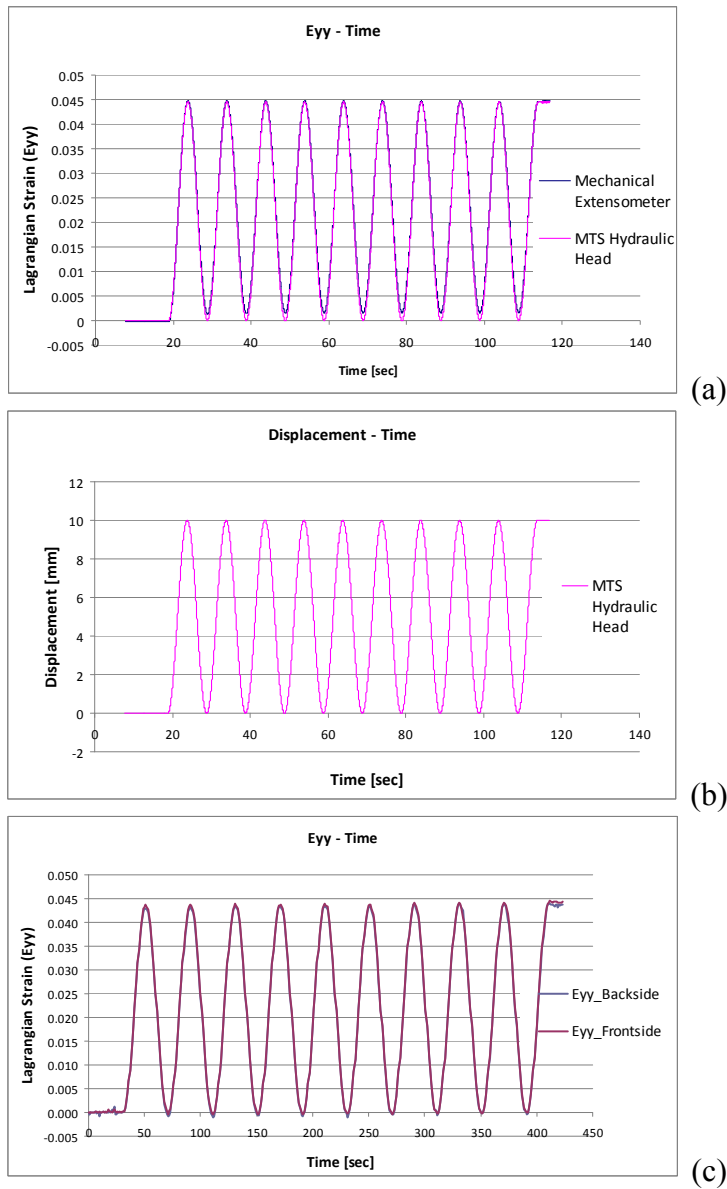


Figure 4.10 : Test results for the silicone bar and mechanical extansometer test

4.2.3 Underwater correlation accuracy tests

Even if verification experiments, previously held, is enough to prove the accuracy of digital image correlation systems, since arterial wall tests will be held in saline solution (0.9% NaCl), in addition to open-atmosphere tests some extra tests should be done to see the effect of diffraction of saline solution and wall thickness and/or flatness of the glass. Aquarium is filled with saline solution to disregard frictions between the arterial wall and base surface. In saline solution arterial wall have almost compensated buoyancy. Experimental setup for underwater experiment is shown in Figure 4.12.

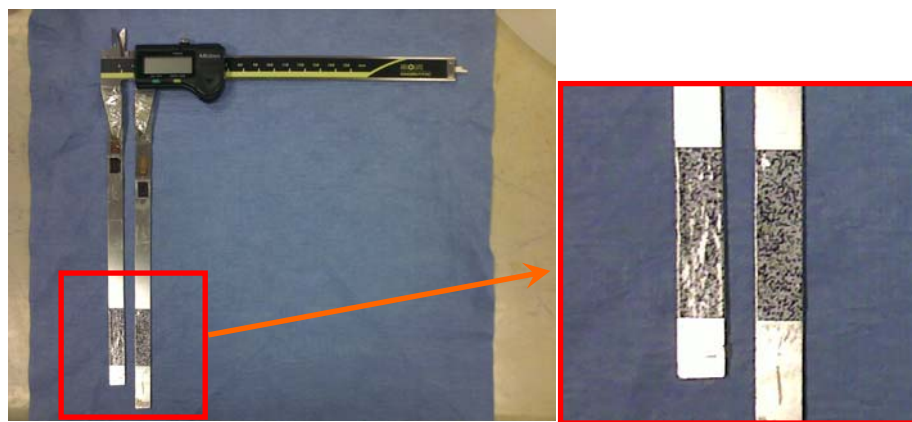


Figure 4.11 : Steel plates fixed to the jaws of the caliper and speckles in detail.

In this experiment two stainless steel plates are fixed to the fixed and sliding jaws of the digital caliper. After fixation, speckled stickers are glued to each plate and covered with polymer film to ensure waterproofness. Sliding jaw is smoothly moved and value on the digital display of the caliper is recorded for each shot taken on the cameras manually.

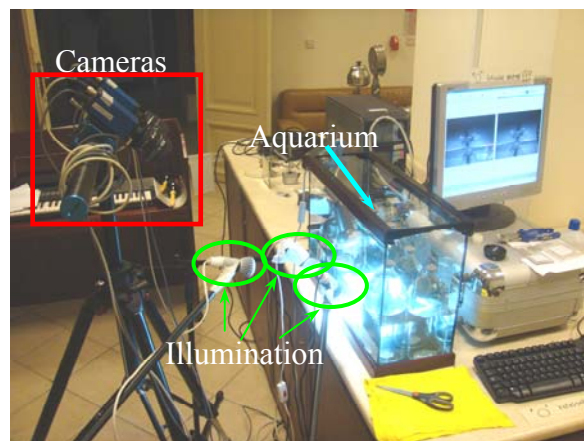


Figure 4.12 : Underwater image correlation test setup.

Assuming that flatness of the glass is high, obtaining high accuracy on displacement results between digital image correlation and caliper values and also calculating zero (or negligible) strain components on each speckled plate since there is no load which will result in any deformation is expected.

Example views from experiment can be seen below in Figure 4.13.

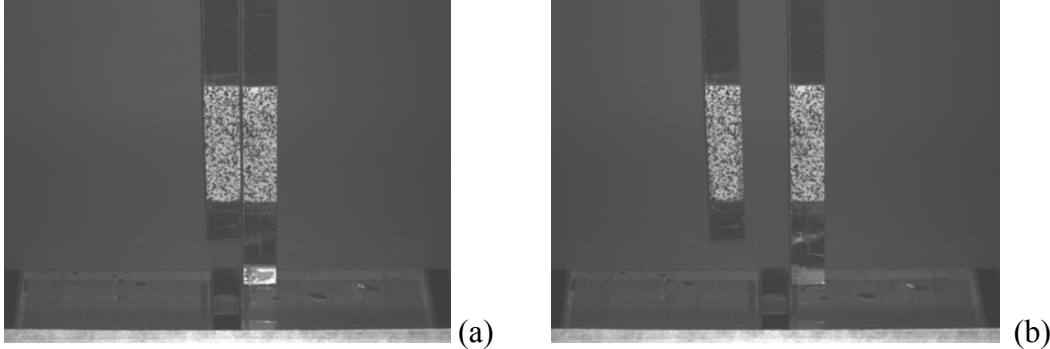


Figure 4.13 : Setup for underwater optical correlation test. (a) Initial view of speckled steel plates, (b) Speckled plates after sliding motion.

In the following figures the results of digital image correlation in water are shown. In Figure 4.14 displacement values obtained by using caliper display and optical correlation in compared. In Figure 4.15a-b E_{xx} and E_{yy} values for steel plates connected to fixed jaw (a) and sliding jaw (b) of the caliper respectively are shown. The strain result in (a) and (b) are digital noise and they were expected to be zero. Thus, the noise of the optical measurement system for underwater measurement setup is around 0.2%. As a result, these results shows that optical correlation systems can be used for also in underwater measurement with acceptable accuracy.

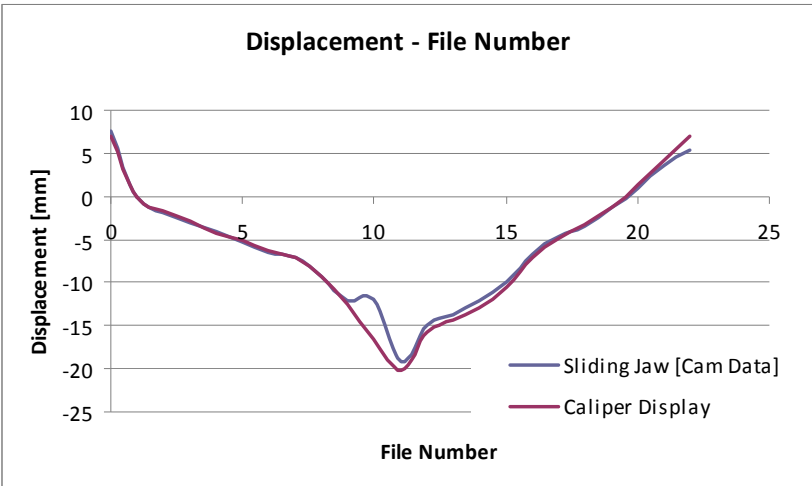
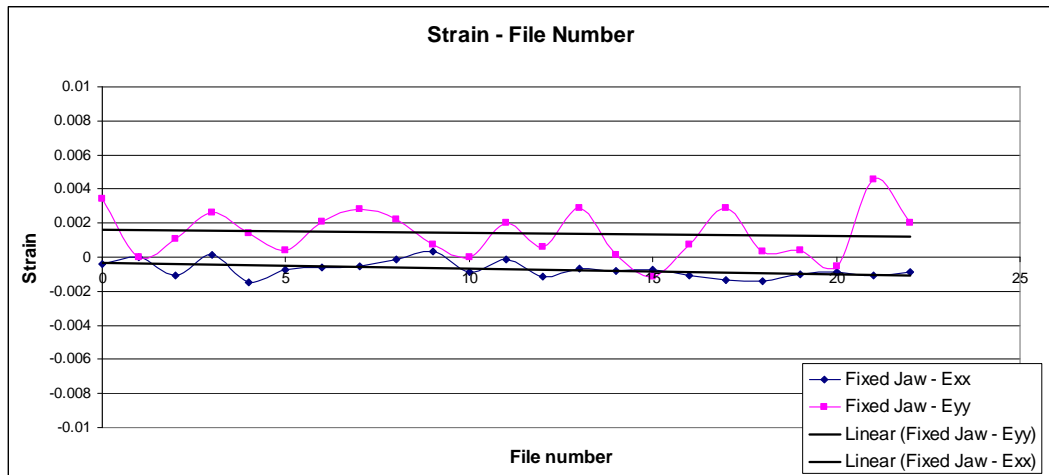
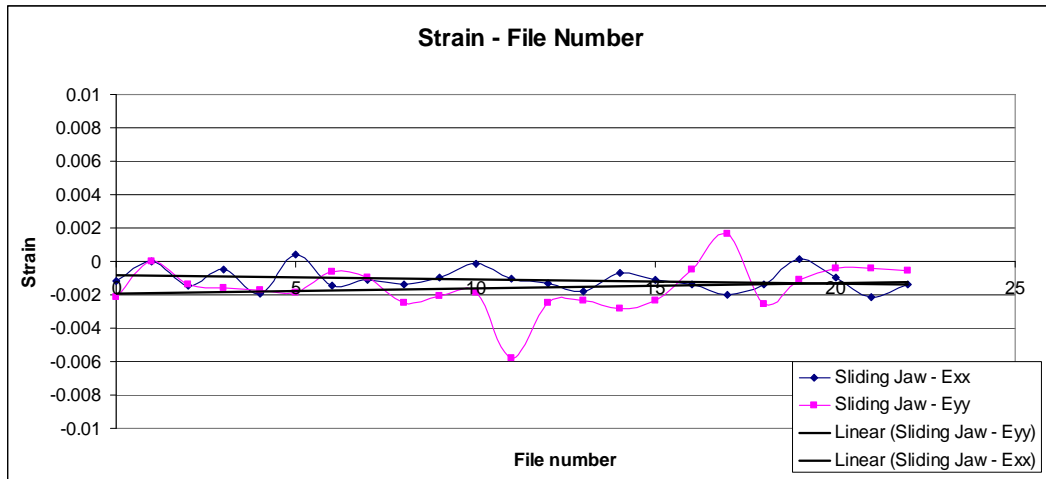


Figure 4.14 : Displacement results of underwater correlation accuracy tests.



(a)



(b)

Figure 4.15 : Strain results of underwater correlation accuracy tests.

4.2.4 Opening angle – test on engineering silicone

Up to this point all previous test were mainly focused on the optical correlation method. Depending on the result of these tests digital image correlation systems can give highly accurate results when compared to conventional measurement systems.

The artery is considered as a cylindrical tube whose wall material is homogeneous and cylindrically orthotropic [53]. Under this hypothesis, at the removal of residual stress from the unloaded state, the vessel wall should become a sector of constant curvature and thickness. If one assumes that both the intact configuration and the open sector are perfectly cylindrical, and that the closing motion involves pure bending, the residual strains in the intact state can be derived as a function of the open sector geometry (the opening angle and radii) [54].

In this experiment same silicon bar in mechanical extensometer test will be used to check the accuracy of theoretical assumptions towards determining residual strains on arterial wall as a beam bending (closing and opening) problem. As explained in pure bending assumption above, silicon bar is bend and tips are attached to each other to represent arterial ring segment. After forming silicone bar as a ring, which is determined as closed-reference configuration, tips will be separated similar to radial cut which was introduced to arterial walls.

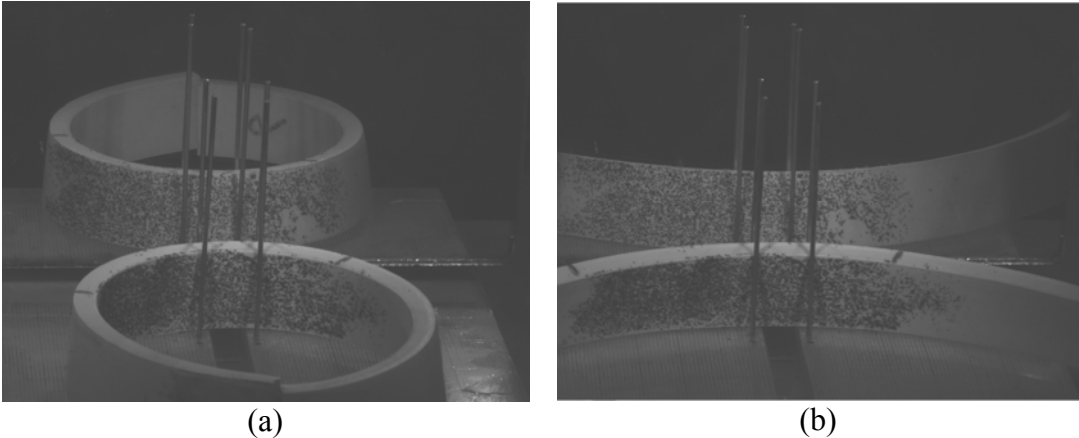


Figure 4.16 : Shots from silicon bar bending tests.

Figures above (a) and (b) showing the bend bar at initial time and after the “cut” in order.

Results are expected to be at same absolute values of strain at inside and outside of the bar, with opposite signs, with respect to assumption of silicon bar’s isotropic structure. These strain results extracted from digital image correlation system and then the pure bending theory will be compared to experimental results.

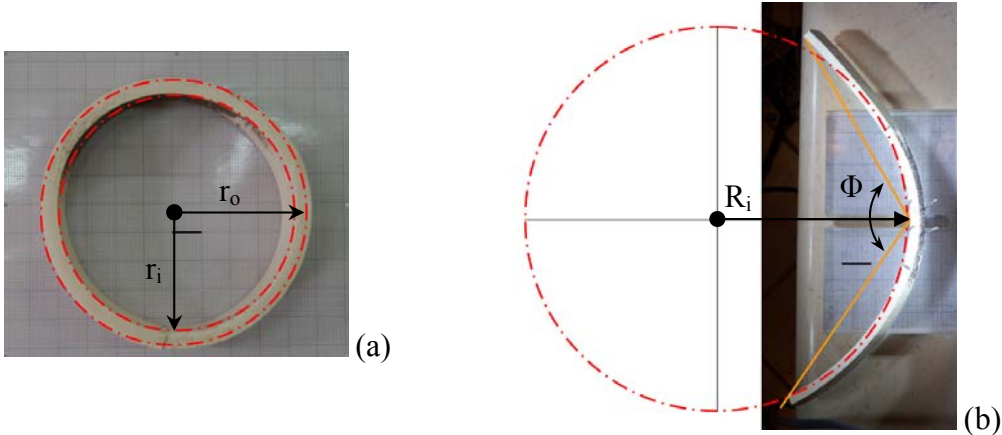


Figure 4.17 : Bended silicon bar, (a) close configuration and (b) open configuration.

On the contrary theoretical result involves a manual data processing procedure. Specimen is photographed from top on a grided paper before and after the cut. r_i and r_o values, which are the inner and outer diameters respectively, are measured from the photo before the cut (4.17a). From the photo, which is taken after the cut (4.17b), R_i and Φ values are obtained. Scaling is an important issue for obtaining precise results and each photo is individually scaled to measure precisely by using the grided paper.

By using reverse formulation method in Section 3.4 strain and stretch values are calculated and compared.

First figure on the following shows the strain result derived from Vic-3D. Horizontal axis shows the file number and vertical axis show Lagrangian strain on exterior surfaces of the bar. On file number 0 and 1 specimen is in closed (reference) configuration which can be understood from strain values. On file number 2 and 3 silicone bar is in open (current) configuration. As estimated the absolute values of strain results for exterior surfaces are approximately the same.

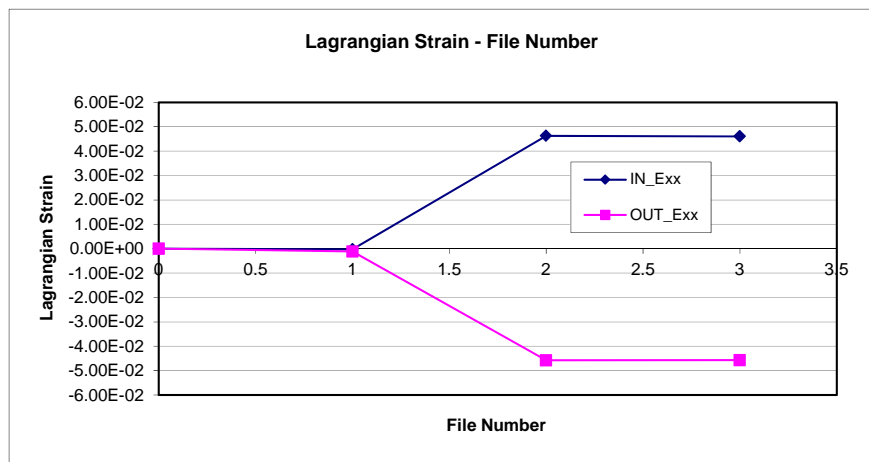


Figure 4.18 : Strain results for the inner and outer surfaces of silicone bar.

Table 4.1 shows the theoretical and experimental result for bending of a silicon bar. Error values between inside and outside of specimen obtained by experiments is 0.8 %. Error values between experimental and theoretical stretch ratio results are 0.3% for inside and 1.5% for outside. Considering the error values, experimental and theoretical result shows that the theory classical way of calculating strains give acceptable results as long as the specimen obeys the assumptions made.

Table 4.2: Stretch ratio results for silicon bar, depending on both theoretical results and camera data.

Specimen Code	t=0 min		t=1 min		r(Ri) [mm]	r(Ro) [mm]	THEO (t=5min)		CAM (t=5min)	
	ri [mm]	ro [mm]	Ri1 [mm]	Φ 1 [deg]			Λ _IN	Λ _OUT	Λ _IN	Λ _OUT
Silicon 01	80	90	252	120	80	90.074	1.05	0.97	1.046	0.954

4.2.5 Underwater arterial wall tests

All of the previous tests's outcomes have partial and/or full importance on accuracy of this final experiment. To sum up; with the experiments which were held out of water helped us to estimate the accuracy range of digital image correlation systems when they are compared to mechanical measurement systems. Then an underwater test is done to see the effect of refraction caused by glass's wall thickness and saline solution. That test also result in acceptable range of accuracy. The last test was the pure bending of a silicon bar and this test proved the validity of theory as "closing of a cylindrical sector" problem.

Consequently strains derived from digital image correlation system has been seen to have adequate accuracy for performing underwater tests.

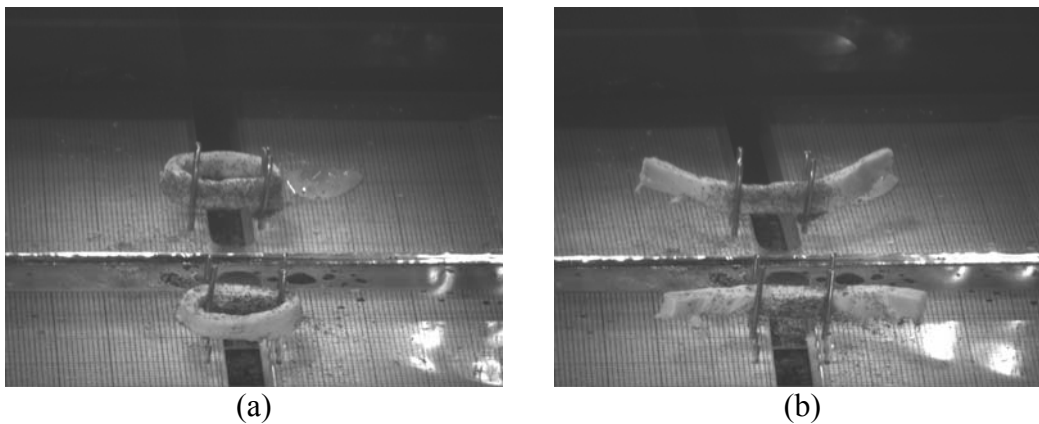


Figure 4.19 : Example shots from stress relieving radial cut tests.

In these test ovine and porcine arteries will be used as specimens. A ring shaped artery (Height:5mm±1mm, diameter as harvested) will be cut in radial direction. Each specimen is speckled carefully and placed in aquarium filled with saline solution(0.9% NaCl). Regarding the observations of Rachev et. all the effect of temperature is disregarded [55]. Since it has no significant effect, test were conducted in room temperature. To prevent rolling of the arterial wall in open configuration, arteries are placed between steel rods, freely. Cameras will shoot from the initial contidion (t=0min) to thirty minutes of time (t=30min). Photos, from front

and top, are taken at $t=0\text{min}$, $t=5\text{min}$, $t=10\text{min}$, $t=15\text{min}$ and $t=30\text{min}$ respectively. Same data processing procedure is carried out as in engineering silicone bending experiment.

Even if arterial wall has a multi-layered structure in this study it will be assumed as a single layered structure; since we only consider comparison of the strains on exterior surfaces.

In the previous figure an arterial ring segment at initial time (4.20a) and after radial cut (4.21b) can be seen.

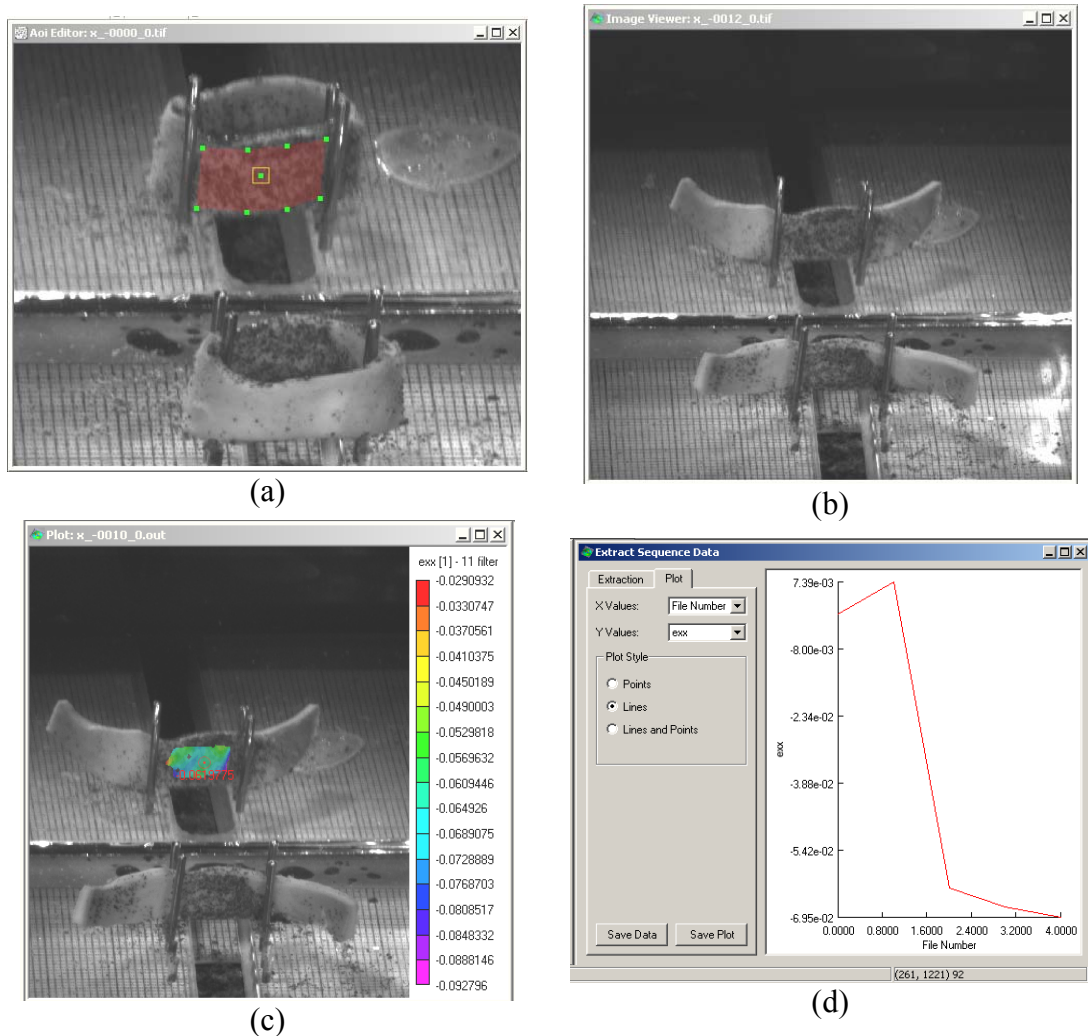


Figure 4.20 : Shots from Vic-3D workspace during arterial wall correlation test.

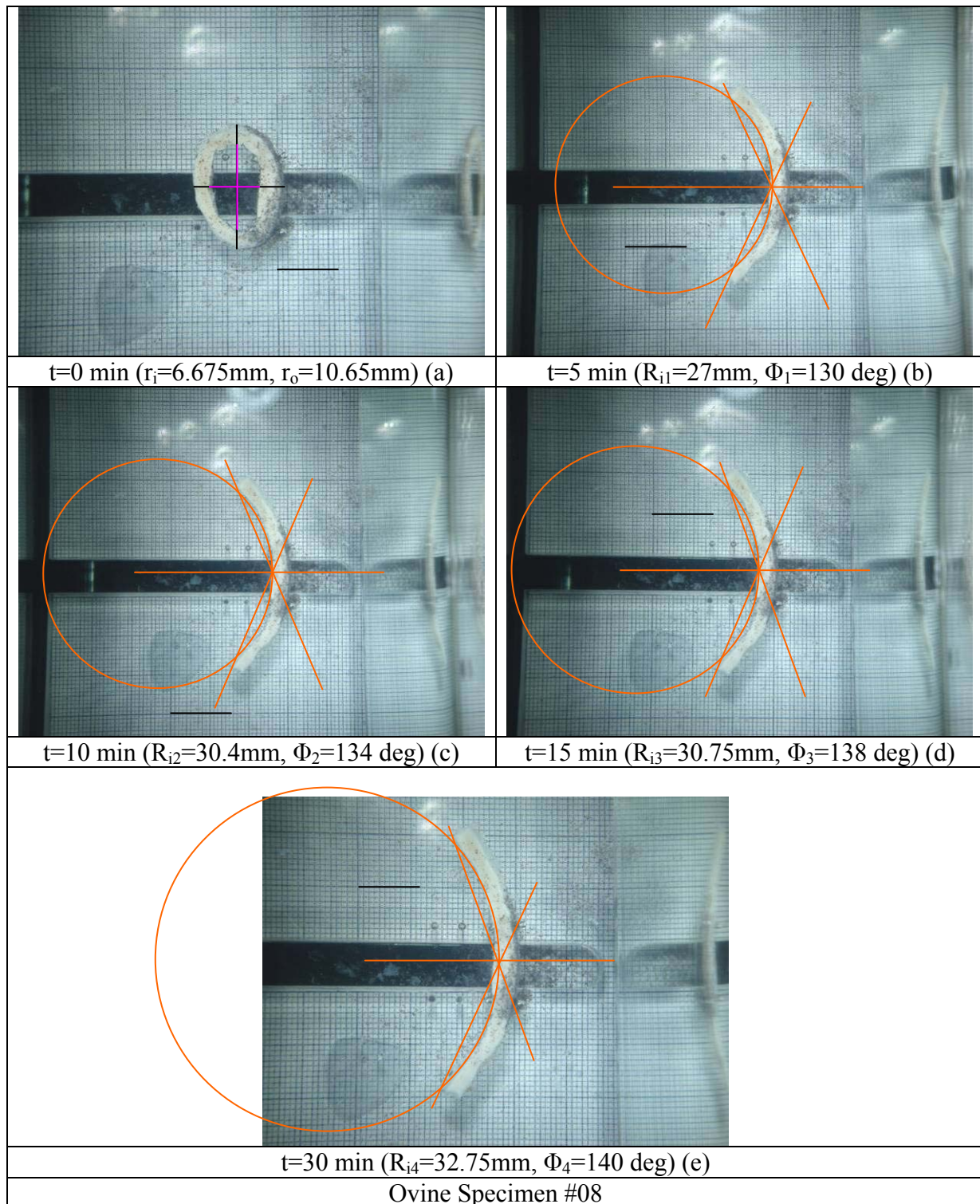


Figure 4.21 : Example photos from the top of an ovine arterial wall specimen at different times.

In tables 4.3, 4.4 and 4.5 the results of underwater arterial wall tests are presented. In these tables,

- Inner and outer diameter values in close configuration,
- Inner diameter and opening angle values in open configuration at every time step, which were measured and
- Stretch ratio results for arterial wall bar, depending on both theoretical results and experimental results
- Strain results for arterial wall bar, depending on both theoretical results and experimental results at every time step, which were calculated and

In addition to data presented above, mean error charts are given at the end of this section.

In specimen column O stands for “*Ovine* - Lamb”, and P stands for “*Porcine* - Pig”

To comment on the results and the error values, there is a significant difference between experimental results and theoretical assumption results.

This difference may cause from:

- Assuming arterial wall as a one layered model. With this assumption partial effects of individual layers are disregarded.
- Optical correlation of a soft tissue underwater is an advanced problem in optical correlation from speckle generation to diffractions.

Result of this study can be interpreted not only as the lacking of the theory, but also in spite of the high error order, which is approximately 50%, for the exterior surfaces of arterial wall may also be interpreted as satisfactory due to order or deformations.

Table 4.3: Initial diameter values and diameter and opening angle values at each time step

Specimen	t=0 min		t=5 min		t=10 min		t=15 min		t=30 min	
	ri [mm]	ro [mm]	Ri1 [mm]	Φ1 [deg]	Ri2 [mm]	Φ2 [deg]	Ri3 [mm]	Φ3 [deg]	Ri4 [mm]	Φ4 [deg]
O8	6.675	10.65	27	130	30.4	134	30.75	138	32.75	140
O9	6.36	9.275	15.375	102	15.95	104	16.79	106	18.45	111
O10	5.75	8.5	13.26	92	13.5	98	13.77	102	14.5	104
O11	7.315	10.725	12.95	65	13.735	75	14.025	78	15.115	85
O12	7	10.15	22.5	118	23.635	120	25.5	125	28.8	130
O13	7.35	10.255	13.875	83	14.91	85	15.275	87	16.2	88
O14	7.2	9.5	15.6	95	16.33	97	17.22	101	18.6	107
P1	6.09	8.775	12	75	12.65	79	12.365	82	13.2	83
P3	6.695	9.79	38.12	140	39.6	145	40	143	46.62	150
P6	6.335	9.225	24.28	122	25.14	126	26.6	130	28.355	133

Table 4.4: Stretch ratio results for arterial wall, depending on both theoretical results and experimental results.

Specimen	r(Ri)	r(Ro)	THEO (t=5min)		CAM (t=5min)		r(Ri)	r(Ro)	THEO (t=10min)		CAM (t=10min)		r(Ri)	r(Ro)	THEO (t=15min)		CAM (t=15min)		r(Ri)	r(Ro)	THEO (t=30min)		CAM (t=30min)	
			Λ_{IN}	Λ_{OUT}	Λ_{IN}	Λ_{OUT}			Λ_{IN}	Λ_{OUT}	Λ_{IN}	Λ_{OUT}			Λ_{IN}	Λ_{OUT}	Λ_{IN}	Λ_{OUT}			Λ_{IN}	Λ_{OUT}	Λ_{IN}	Λ_{OUT}
			O8	6.675	10.420	1.124			0.826	1.036	0.950	6.675			10.505	1.164	0.836	1.038			0.938	6.675	10.261	1.075
O9	6.360	9.109	1.048	0.870	1.024	0.960	6.360	9.127	1.059	0.873	1.026	0.956	6.360	9.175	1.085	0.883	1.030	0.955	6.360	9.216	1.112	0.889	1.033	0.957
O10	5.750	8.510	1.127	0.920	1.015	0.966	5.750	8.386	1.070	0.883	1.027	0.963	5.750	8.316	1.038	0.861	1.027	0.958	5.750	8.362	1.065	0.871	1.025	0.951
O11	7.315	10.833	1.131	0.965	1.017	0.958	7.315	10.721	1.095	0.933	1.018	0.958	7.315	10.691	1.086	0.924	1.018	0.959	7.315	10.680	1.091	0.915	1.019	0.953
O12	7.000	10.062	1.107	0.878	1.054	0.943	7.000	10.097	1.125	0.884	1.050	0.941	7.000	10.056	1.113	0.871	1.049	0.944	7.000	10.107	1.143	0.878	1.047	0.939
O13	7.350	10.100	1.017	0.895	1.047	0.956	7.350	10.208	1.071	0.921	1.053	0.952	7.350	10.210	1.074	0.920	1.052	0.950	7.350	10.317	1.127	0.946	1.054	0.947
O14	7.200	9.393	1.023	0.900	1.053	0.948	7.200	9.430	1.046	0.911	1.055	0.951	7.200	9.430	1.050	0.908	1.057	0.951	7.200	9.417	1.048	0.900	1.051	0.936
P1	6.090	8.882	1.149	0.964	1.016	0.937	6.090	8.902	1.166	0.967	1.014	0.945	6.090	8.784	1.105	0.933	1.015	0.942	6.090	8.898	1.168	0.962	1.022	0.939
P3	6.695	9.969	1.265	0.919	1.045	0.947	6.695	9.713	1.150	0.855	1.058	0.932	6.695	9.884	1.228	0.896	1.046	0.929	6.695	9.722	1.161	0.852	1.067	0.928
P6	6.335	9.383	1.235	0.933	1.091	0.940	6.335	9.286	1.191	0.906	1.100	0.937	6.335	9.228	1.166	0.888	1.111	0.933	6.335	9.225	1.169	0.884	1.119	0.930

Table 4.5: Strain results for arterial wall, depending on both theoretical results and experimental results.

Specimen	r(Ri)	r(Ro)	THEO (t=5min)		CAM (t=5min)		r(Ri)	r(Ro)	THEO (t=10min)		CAM (t=10min)		r(Ri)	r(Ro)	THEO (t=15min)		CAM (t=15min)		r(Ri)	r(Ro)	THEO (t=30min)		CAM (t=30min)	
			E_{IN}	E_{OUT}	E_{IN}	E_{OUT}			E_{IN}	E_{OUT}	E_{IN}	E_{OUT}			E_{IN}	E_{OUT}	E_{IN}	E_{OUT}			E_{IN}	E_{OUT}	E_{IN}	E_{OUT}
			O8	6.675	10.420	0.124			-0.174	0.036	-0.050	6.675			10.505	0.164	-0.164	0.038			-0.062	6.675	10.261	0.075
O9	6.360	9.109	0.048	-0.130	0.024	-0.040	6.360	9.127	0.059	-0.127	0.026	-0.044	6.360	9.175	0.085	-0.117	0.030	-0.045	6.360	9.216	0.112	-0.111	0.033	-0.043
O10	5.750	6.374	0.127	-0.080	0.015	-0.034	5.750	8.386	0.070	-0.117	0.027	-0.037	5.750	8.316	0.038	-0.139	0.027	-0.042	5.750	8.362	0.065	-0.129	0.025	-0.049
O11	7.315	10.833	0.131	-0.035	0.017	-0.042	7.315	10.721	0.095	-0.067	0.018	-0.042	7.315	10.691	0.086	-0.076	0.018	-0.041	7.315	10.680	0.091	-0.085	0.019	-0.047
O12	7.000	10.062	0.107	-0.122	0.054	-0.057	7.000	10.097	0.125	-0.116	0.050	-0.059	7.000	10.056	0.113	-0.129	0.049	-0.056	7.000	10.107	0.143	-0.122	0.047	-0.061
O13	7.350	10.100	0.017	-0.105	0.047	-0.044	7.350	10.208	0.071	-0.079	0.053	-0.048	7.350	10.210	0.074	-0.080	0.052	-0.050	7.350	10.317	0.127	-0.054	0.054	-0.053
O14	7.200	9.393	0.023	-0.100	0.053	-0.052	7.200	9.430	0.046	-0.089	0.055	-0.049	7.200	7.558	0.050	-0.092	0.057	-0.049	7.200	9.417	0.048	-0.100	0.051	-0.064
P1	6.090	8.882	0.149	-0.036	0.016	-0.063	6.090	8.902	0.166	-0.033	0.014	-0.055	6.090	8.784	0.105	-0.067	0.015	-0.058	6.090	8.898	0.168	-0.038	0.022	-0.061
P3	6.694	7.374	0.265	-0.081	0.045	-0.053	6.694	9.711	0.150	-0.145	0.058	-0.068	6.69	9.88	0.228	-0.104	0.046	-0.071	6.694	9.720	0.161	-0.148	0.067	-0.072
P6	6.334	6.962	0.235	-0.067	0.091	-0.060	6.334	6.962	0.191	-0.094	0.100	-0.063	6.334	9.229	0.166	-0.112	0.111	-0.067	6.334	9.226	0.169	-0.116	0.119	-0.070

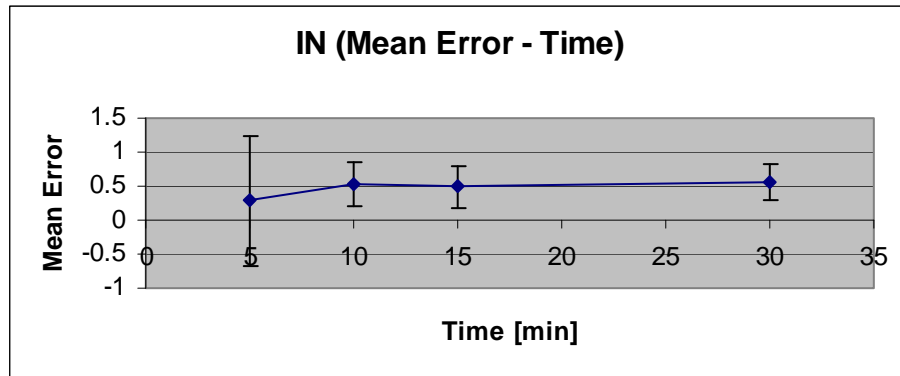


Figure 4.22 : Mean Error – Time graph for inside of arterial wall

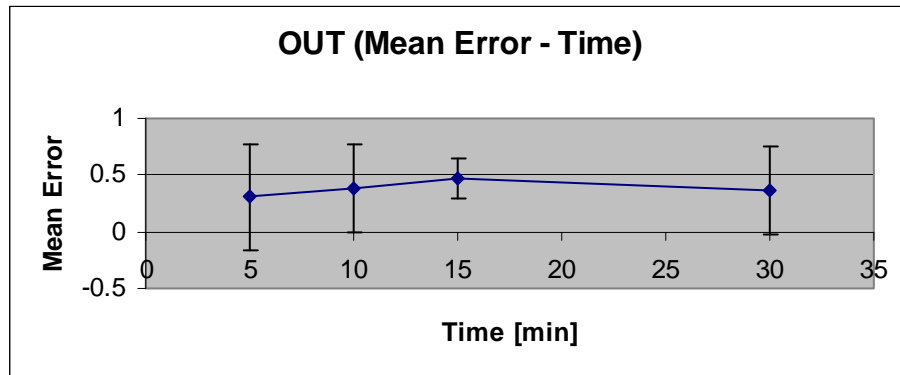


Figure 4.23 : Mean Error – Time graph for outside of arterial wall

5 CONCLUSION AND REMARKS

The major purpose of this research was to measure the residual strains inner and outer layers of arterial vessel and then compare it to common theoretical assumptions on this problem. One of the advanced non-contacting measurement method, optical correlation system is used to measure the deformation field on arterial specimens.

Various verification test is conducted to check the error order of optical correlation systems for this study.

A novel experimental setup has been established for measurement of residual strains on an arterial wall at room temperature.

As it is previously noted; mechanical behaviour of arterial walls varies from site to site in same body. Specimen selection should be carried out with respect to this to get a higher reliability of the experiment.

The difference between experimental and theoretical results may cause from:

- Assuming arterial wall as if it is one layered. With this assumption partial effects of individual layers are disregarded.
- Optical correlation of a soft tissue underwater is an advanced problem in optical correlation from speckle generation to diffractions.

When the results are considered, a significant difference between theoretical and experimental results revealed. This will surely trigger future studies on the subject.

In future studies some points may be included to the scope

- Effect of compressibility
- Measurement of residual strains through thickness
- Separation of layers and layer specific strain measurements
- Implication of these results to constitutive models in literature

REFERENCES

- [1] **Raghavan, M. L.**, Lecture Notes on Cardiovascular Bio-solid Mechanics, Department of Biomedical Engineering University of Iowa.
- [2] **Junquera, L.C., Carneiro, J.**, 2005, Basic Histology 11th Edition – Text and atlas, McGraw-Hill.
- [3] **Mescher, A. L.**, 2010, Junquera's Basic Histology 12th Edition – Text and atlas, McGraw-Hill.
- [4] **Bronzino, J. D.**, 2006. The Biomedical Engineering Handbook, Taylor – Francis Group.
- [5] **Fung, Y.C.**, 1993. Biomechanics. Mechanical Properties of Living Tissues, Springer-Verlag, New York, 2nd edition.
- [6] **Kalita, P., Schaefer, R.**, 2008. Mechanical Models of Artery Walls, *Arch Comput Methods Eng*, **15**: 1–36.
- [7] **Hayashi, K.**, 2003. Mechanical properties of soft tissues and arterial walls, Biomechanics of soft tissue in cardiovascular systems, In: Holzapfel GA, Ogden RW (Eds) Biomechanics of soft tissue in cardiovascular systems. Springer, New York, pp 15–64.
- [8] **Holzapfel, G.A., Gasser, T.C., Ogden, R.W.**, 2000. A new constitutive framework for arterial wall mechanics and a comparative study of material models, Institute for Structural Analysis, Computational Biomechanics Graz University of Technology, Schiesstattgasse 14B, A-8010 Graz, Austria.
- [9] **Humphrey, J.D., Na, S.**, 2002. Elastodynamics and Arterial Wall Stress, *Annals of Biomedical Engineering*, **30**:509–523.
- [10] **Rhodin, J.A.G.**, 1980. Architecture of the vessel wall. In H. V. Sparks Jr. D. F. Bohr, A. D. Somlyo and S. R. Geiger, Editors, Handbook of Physiology, the Cardiovascular System, **2**:1-31. American Physiology Society, Bethesda, Maryland.
- [11] **B.S. Schulze-Jane**, 1939. Über die schraubenförmige Struktur der arterienwand. *Gegenbauers Morphol. Jahrbuch*, **83**:230-246.
- [12] **J. Staubesand**, 1959. Anatomic der Blutgefäße, I. Funktionelle Morphologie der Arterien, Venen und arterio-venösen Anastomosen. In M. Ratschow, editor, Anilogy, Chapter 2, pp 23-82. Thieme, Stuttgart.
- [13] **Holzapfel, G.A.**, 2003. Structural and numerical models for the (visco)elastic response of arterial walls with residual stresses. In: Holzapfel GA, Ogden RW (Eds) Biomechanics of soft tissue in cardiovascular system. Springer, New York, pp 109–184.

- [14] **J. D. Humphrey**, 2002. Cardiovascular Solid Mechanics, Springer-Verlag, New York, Inc. .
- [15] **G. A. Holzapfel**, 2000. Nonlinear Solid Mechanics; A continuum Approach for Engineering.
- [16] **Reddy, J. N.**, 2008. An Introduction to Continuum Mechanics, Cambridge University Press.
- [17] **Lubarda, V.A.**, 2002. Elastoplasticity Theory, CRC Press.
- [18] **Schneck, D.J.**, 2000. The Biomedical Engineering Handbook. Soft tissue modeling. CRC Press LLC, 2nd edition.
- [19] **Silver, F.H., Christiansen, D.L. and Buntin, C.M.**, 1989. Mechanical properties of the aorta: A review. *Critical Reviews in Biomed. Engr.*, **17**:323–358.
- [20] **Martin, R.B., Burr, D.B., and Sharkey, N.A.**, 1998. Skeletal Tissue Mechanics, Springer-Verlag, New York.
- [21] **Woo, S.L.Y., Gomez, M.A., and Akeson, W.H.**, 1985. Mechanical behaviors of soft tissues: Measurements, modifications, injuries and treatment. In *The Biomechanics of Trauma*, A. M. Nahum and J. Melvin (Eds), Norwalk, Appleton Crofts., 107-133.
- [22] **Holzapfel, G.A.**, 2000. Biomechanics of Soft Tissue, Institute for Structural Analysis, Graz University of Technology.
- [23] **Taber, L.A.**, .2004. Nonlinear Theory of Elasticity – Applications in Biomechanics, World Scientific.
- [24] **Hasegawa, M., Azuma, T.**, 1974. Wall Structure and static viscoelasticities of large veins. *J. Jap. College Angiol.* **14**:87-92.
- [25] **Lanir, Y., Fung, Y.C.**, 1974. Two dimensional properties of rabbit skin *J. Biomech.* **7**:171-182.
- [26] **Tong, P., Fung, Y.C.**, 1976. The stress-strain relationship for the skin. *J. Biomech.* **9**:649-657.
- [27] **Ridge, M.D., Wright, V.**, 1966. The directional effect of skin – A bioengineering study of skin with particular reference to Langer’s lines.
- [28] **Woo, S.L.Y., Lubock, P., Gomez, M.A., Jemmott, G.F., Kuei, S.C., Akenson, W.H.**, 1979. Large deformation nonhomogeneous and directional properties of articular cartilage. *Journal of Biomechanics*, **12**(6):437-446
- [29] **Chuong, C. J., and Fung, Y. C.**, 1984. Compressibility and constitutive equation of arterial wall in radial compression experiments. *J. Biomech.*, **17**:35-40.
- [30] **Vawter, D.L., Fung, Y.C., West, J.B.**, 1978. Elasticity of excised dog lung parenchyma. *J. Appl. Physiol.* **45**:261-269.
- [31] **Carew, T.E., Vaishnav, R.N. Patel, D.J.**, 1968. compressibility of arterial wall. *Circ. Res.* **23**:61-68.

- [32] **Lallir, Y., Fung, Y.C.**, 1974. Two-dimensional mechanical properties of rabbit skin-I. Experimental system, *J. Biomech.*, 7:29-34.
- [33] **Deng, S.X., Tomioka, J., Debes, J.C., Fung, Y.C.**, 1994. New experiments on shear modulus of elasticity of arteries, *Am. J. Physiology*, **266**:HI-HI0.
- [34] **Chuong, C. J., and Fung, Y. C.**, 1986. On Residual Stresses in Arteries, *J. Biomech. Eng.*, **108**:189–192.
- [35] **Johnson, B. E., and Hoger, A.**, 1995, The Use of a Virtual Configuration in Formulating Constitutive Equations for Residually Stressed Elastic Materials, *J. Elast.*, **41**: 177–215.
- [36] **Rachev A., Greenwald S.E.**, 2003. Residual strains in conduit arteries. *J Biomech.*, **36**:661–670
- [37] **Raghavan, M.L., Trivedi, S., Nagaraj, A., Mcpherson, D.D., Chandran, K.B.**, 2004. Three-Dimensional Finite Element Analysis of Residual Stress in Arteries. *Annals of Biomedical Engineering*, **32**(2):,257–263
- [38] **Fung, Y. C.**, 1991. What are the residual stresses doing in our blood vessels? *Ann Biomed. Eng.* **19**:237–249
- [39] **Dyke, T. J.V., Hoger, A.**, 2002, A New Method for Predicting the Opening Angle for Soft Tissues, **124**: 347-354
- [40] **Cardamone, L., Valentín, A., Eberth, J.F., Humphrey, J.D.**, 2009. *Biomech Model Mechanobiology*, **8**:431–446
- [41] **Sutton, M. A., Orteu, J. J., Schreier, H.W.**, 2009. Image Correlation for Shape, Motion and Deformation Measurements, Springer Science+Business Media
- [42] **Url-1** <<http://www.correlatedsolutions.com/index.php/principle-of-digital-image-correlation>>, accessed at 10.02.2011.
- [43] **Peters, W.H., Ranson, W.F.**, 1981. Digital imaging techniques in experimental stress analysis, *Opt. Eng.*, **21**(3): 427–432
- [44] **Sutton, A.M.**, Digital image correlation for Shape and Deformation Measurements, 2008. Springer Handbook of Experimental Solid Mechanics, Ed: William N. Sharpe, W. N. Jr.
- [45] **Vidiik, A., Vuust, J.**, 1978. Biology of Collagen: Proceedings of a Symposium, Aarhus, Academic Press
- [46] **Birk, D. E., Silver, F. H., Trelstad, R.L.**, 1991. Matrix assembly, in Cell Biology of Extracellular Matrix, 2nd Edition, Hay, E. D. (Ed), Plenum Press.
- [47] **Fung, Y.C.**, 1972. Stress-strain history relations of soft tissues in simple elongation, in Biomechanics: It's Foundations and Objectives, Prentice Hall
- [48] **Vawter, D.L., Fung, Y.C., West, J.B.**, 1978. elasticity of excised dog lung parenchyma. *J. Appl. Physiol.*, **45**:261-269
- [49] **Tong, P., Fung, Y.C.**, 1976, The stress-strain relationship for the skin. *J. Biomech.*, **9**:649-657

- [50] **Maruel, W., Wu, Y., Thalmann, N. M., Thalmann, D.,** 1998. Biomechanical Models for Soft Tissue Simulation, Springer.
- [51] **Kwan, M. K., Woo, S.L. –Y.,** 1989. A structural model to describe the nonlinear stress-strain behavior for parallel-fibered collagenous tissues, *J. Biomech. Eng.*, **111**:361-363
- [52] **Masson, I., Boutouyrie, P., Laurent, S., Humphrey, J.D., Zidi, M.,** 2008. Characterization of arterial wall mechanical behavior and stresses from human clinical data, *Journal of Biomechanics*, **41**:2618-2627
- [53] **D. J. Patel and D. L. Fry,** 1969. The elastic symmetry of arterial segments in dogs. *Circ. Res.*, **24**:1-8.
- [54] **Zhou, X., Lu, J.,** 2009. Estimation of vascular open configuration using finite element inverse elastostatic method, *Engineering with Computers* **25**:49–59
- [55] **Rachev, A., Greenwald, S.E.,** 2003. *Residual strains in conduit arteries*, *Journal of Biomechanics* **36**:661–670
- [56] **Vaishnav, R.N., Vossoughi, J.,** 1987. Residual stress and strain in aortic segments. *Journal of Biomechanics* **20**:235–239.
- [57] **Chuong, C.J., Fung, Y.C.,** 1983. Three-dimensional stress distribution in arteries. *Journal of Biomechanical Engineering* **105**:268–274.
- [58] **Bergel, D.H.,** 1960 The viscoelastic properties of the arterial wall. Ph.D., University of London.
- [59] **Greenwald, S.E., Moore, J.E., Rachev, A., Kane, T.C.P., Meister, J.-J.,** 1997. Experimental investigation of residual strains in the artery wall. *Journal of Biomechanical Engineering* **119**, 438–444.
- [60] **Stergiopoulos, N., Vulliamoz, S., Rachev, A., Meister, J.J., Greenwald, S.E.,** 2001. Assessing the homogeneity of the elastic properties and composition of the pig aortic media. *Journal of Vascular Research*, **38**:237–246.
- [61] **Fung, Y. C ,** 1984, *Biodynamics: Circulation*, Springer-Verlag, New York, pp. 59-60.
- [62] **Chuong CJ, Fung YC,** 1986. Residual stress in arteries. In: Schmid-Schonbein GW, Woo SLY, Zweifach BW (eds) *Frontiers in biomechanics*. Springer, New York, pp 117–129

CURRICULUM VITAE

Candidate's full name: Gökhan BAYSAL

Place and date of birth: Istanbul, 31st January 1986

Universities and

Colleges attended: Istanbul Technical University (2009)
Mechanical Engineering

Kadikoy Anatolian Highschool (2004)

Publications:

- Onur Hapa, F. Alan Barber, Emin Sünbuloğlu, Yavuz Kocabey, Nazlı Şarkalkan, **Gökhan Baysal**, “Tendon-grasping strength of various suture configurations for rotator cuff repair” *Knee Surgery, Sports Traumatology, Arthroscopy*, DOI 10.1007/s00167-010-1322-y
- Yavuz Kocabey , Omer Taser, John Nyland, Haluk Ince, Feyzi Sahin, Emin Sunbuloglu, **Gokhan Baysal**, Horizontal Suture Placement Influences Meniscal Repair Fixation Strength, ISAKOS 8th Biennial, May 15-19 2011, Rio De Janerio - Brazil
- Hapa, O., Hüsamettin Çakıcı, Raif Özden, Ahmet Nedim Yanat, **Gökhan Baysal**, Nazlı Şarkalkan, Trombositten zengin plazmanın rotator manşet-kemik iyileşmesi üzerine etkisi, XXII. Ulusal Türk Ortopedi ve Travmatoloji Kongresi, 31 Ekim-5 Kasım 2011, Antalya-Belek, Türkiye
- Ali Şeker, **Gökhan Baysal**, Nafiz Bilsel, Emin Sünbuloğlu, Ergün Bozdağ, Proksimal Femoral Çivileme ile Tedavi Edilmiş İnstabil İntertrokanterik Femur Kırıklarının Sonlu Eleman Yöntemi ile Biyomekanik Analizi, XXII. Ulusal Türk Ortopedi ve Travmatoloji Kongresi, 31 Ekim-5 Kasım 2011, Antalya-Belek, Türkiye